Chapter 3

Results

Characterization of curcumin and curcumin-metal complexes

The interaction between curcumin and some metal ions can be divided into two parts. The first part involves the solution phase which was studied by the following techniques.

- UV-Visible spectroscopy
- Cyclic voltammetry
- Nuclear magnetic resonance spectroscopy

The second part involves studying the solid products (precipitates) that formed when curcumin reacted with Pb^{2+} and Cu^{2+}. These products were studied for their physical properties and elemental compositions and further investigated by the following techniques.

- Infrared spectroscopy
- X-ray fluorescence spectrometry

3.1 UV-Visible absorption spectroscopy

UV-Visible absorption spectroscopy is a technique for studying the electronic transitions of compound. The electronic absorption spectral were recorded in the range of 200-800 nm.

3.1.1 Study of complex between Fe^{3+}, Pb^{2+} and Cd^{2+} and curcumin in aqueous media

In basic media the solution of curcumin exhibit red color. The maximum absorption bands obtained in basic media were observed at 260 nm along with the presence of a shoulder-like band at 360 and 420 nm.

Maximum absorbance values of Pb^{2+} and Cd^{2+} were obtained at 220 nm and 210 nm, respectively, but Fe^{3+} did not show significant absorption in this spectral region.

The composition of curcumin and metal ions was established by the Job's method. In these methods curcumin and metal ions were prepared in the same concentration (1×10^{-4} M). Different amounts of curcumin and metal ions were added to each flask. The absorbances of all the mixed solutions appeared like that of pure curcumin with no new peak. Figure 16 to Figure 18 show spectra of curcumin-Fe^{3+}, curcumin-Pb^{2+} and curcumin-Cd^{2+} system, respectively.

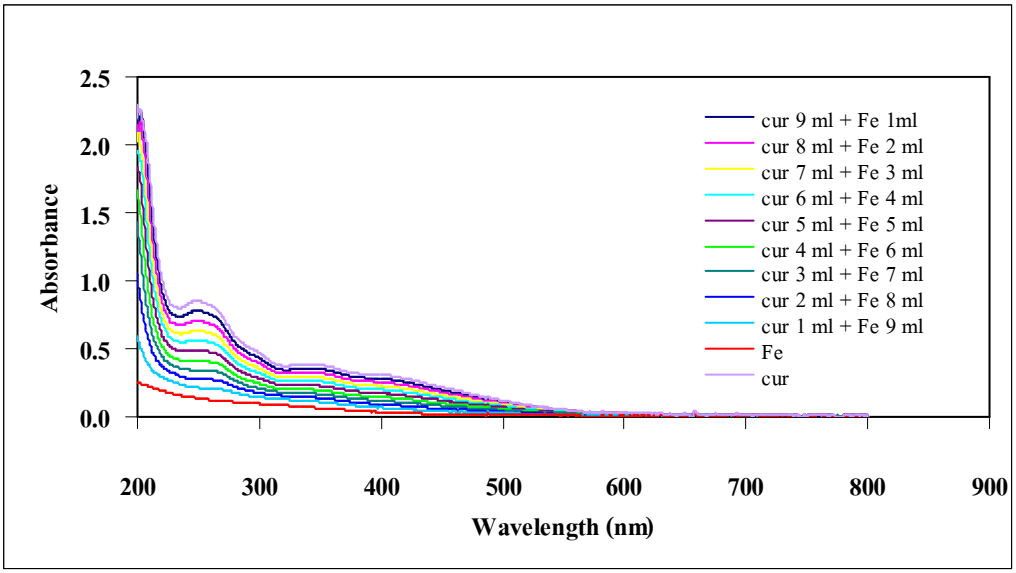

Figure 16 UV-Vis absorption spectra of Fe^{3+}, curcumin and curcumin-Fe^{3+}

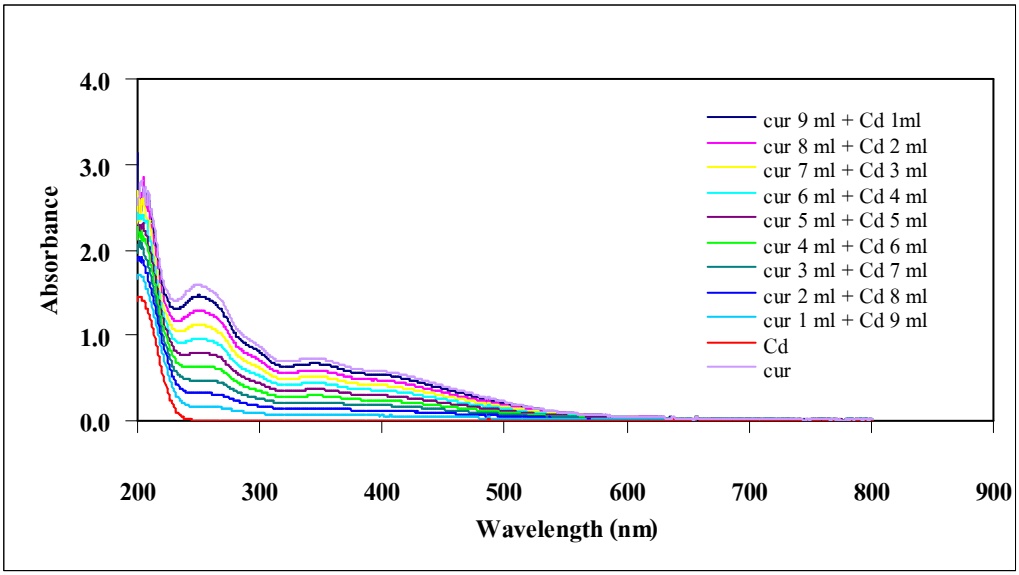

Figure 17 UV-Vis absorption spectra of Pb^{2+}, curcumin and curcumin-Pb^{2+}

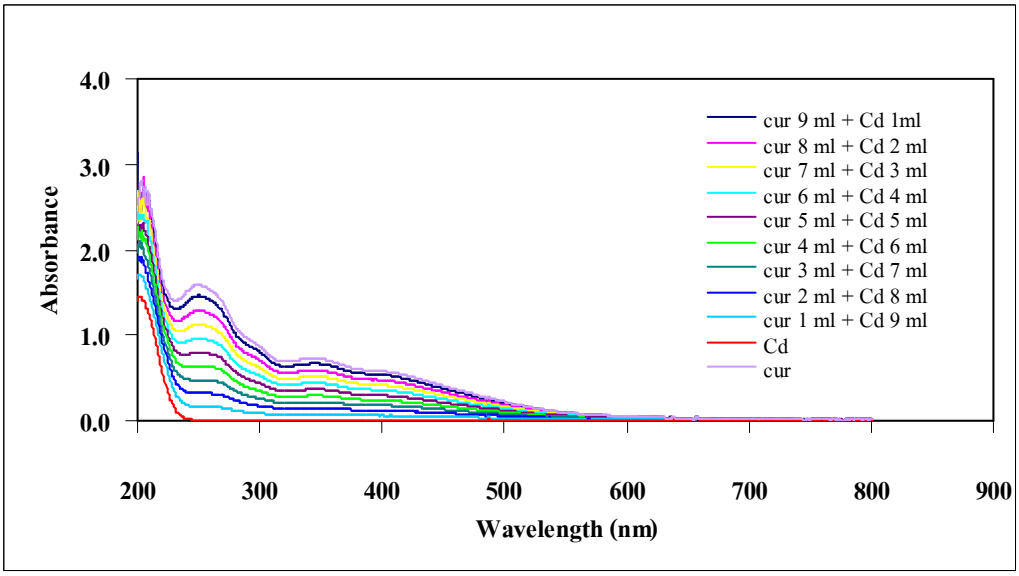

Figure 18 UV-Vis absorption spectra of Cd^{2+}, curcumin and curcumin-Cd^{2+}

3.1.2 Study of interaction between curcumin and metal ions (Fe^{3+}, Pb^{2+}, Cd^{2+}, Mn^{2+}, Bi^{2+} and Cr^{3+}) in 50% methanol media

The maximum absorption bands of curcumin were observed at 420 nm along with the presence of a shoulder-like band at 260 and 360 nm.

Maximum absorbance value of Pb^{2+} were observed at 220 nm but Bi^{2+}, Fe^{3+} and Cr^{3+} at 204 nm. Mn^{2+} and Cd^{2+} did not show significant absorption in this spectral region.

When Fe^{2+} was added to curcumin solutions, the bands of curcumin did not shift and no new band was observed. Similar results were obtained with the other metal ions. The UV-Vis spectra of curcumin, metal ion, and curcumin-metal ion (Fe^{3+}, Pb^{2+}, Cd^{2+}, Mn^{2+}, Bi^{2+} and Cr^{3+}) are shown in Figure 19 to Figure 24.

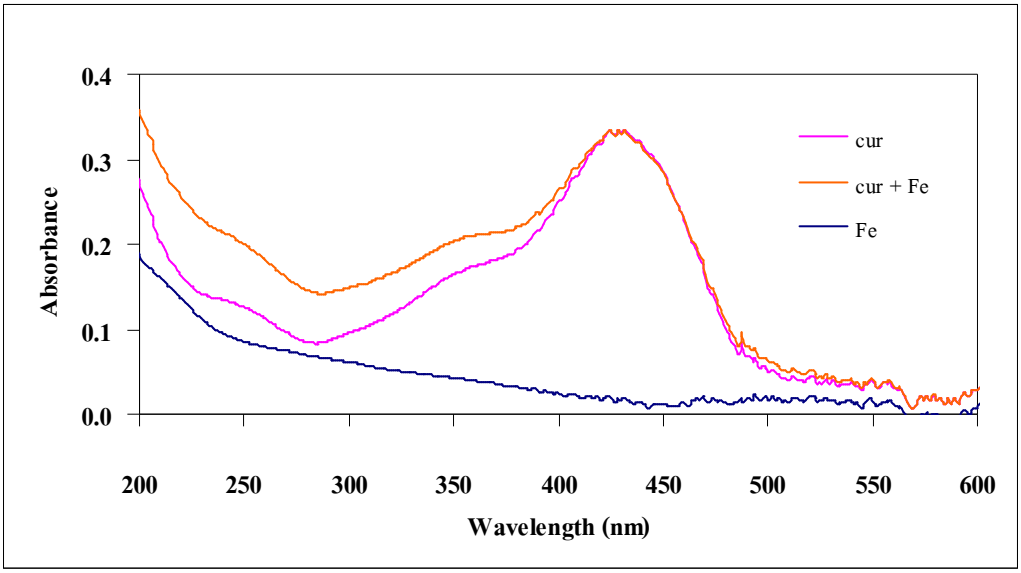

Figure 19 UV-Vis absorption spectra of Fe^{3+}, curcumin and curcumin-Fe^{3+}

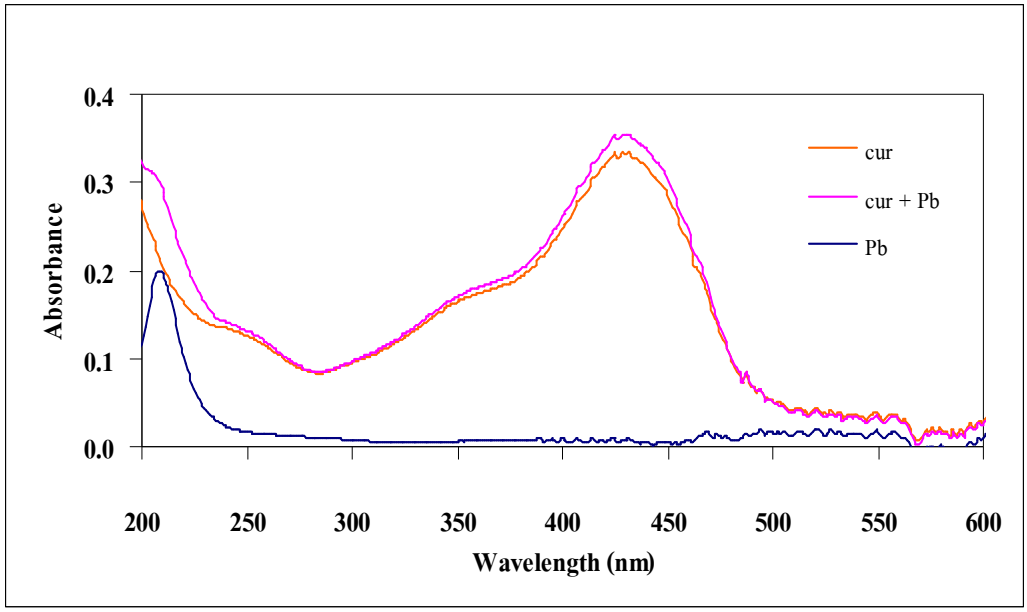

Figure 20 UV-Vis absorption spectra of Pb^{2+}, curcumin and curcumin-Pb^{2+}

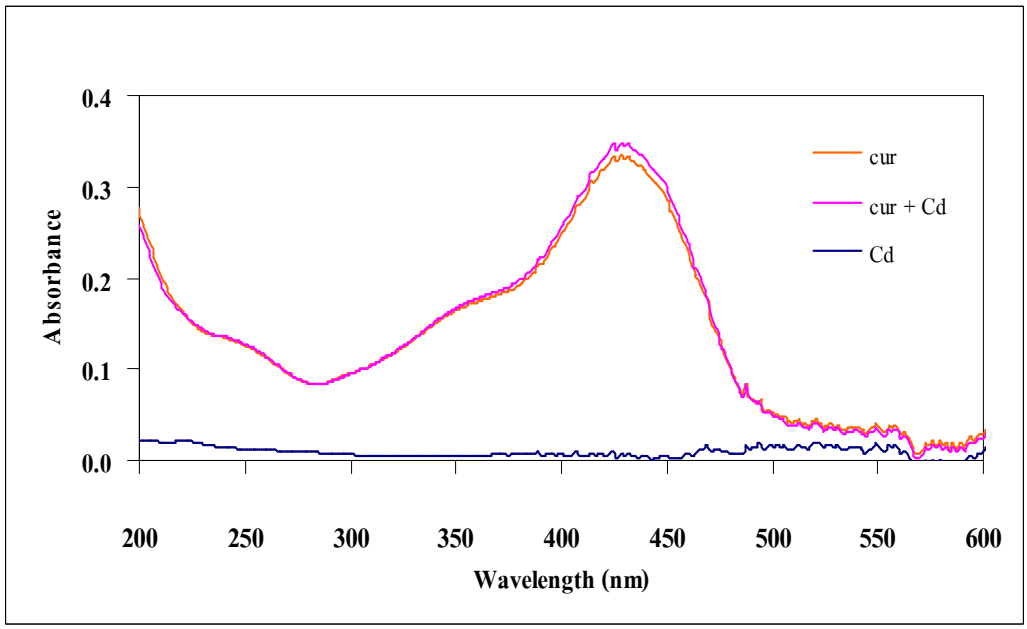

Figure 21 UV-Vis absorption spectra of Cd^{2+}, curcumin and curcumin-Cd^{2+}

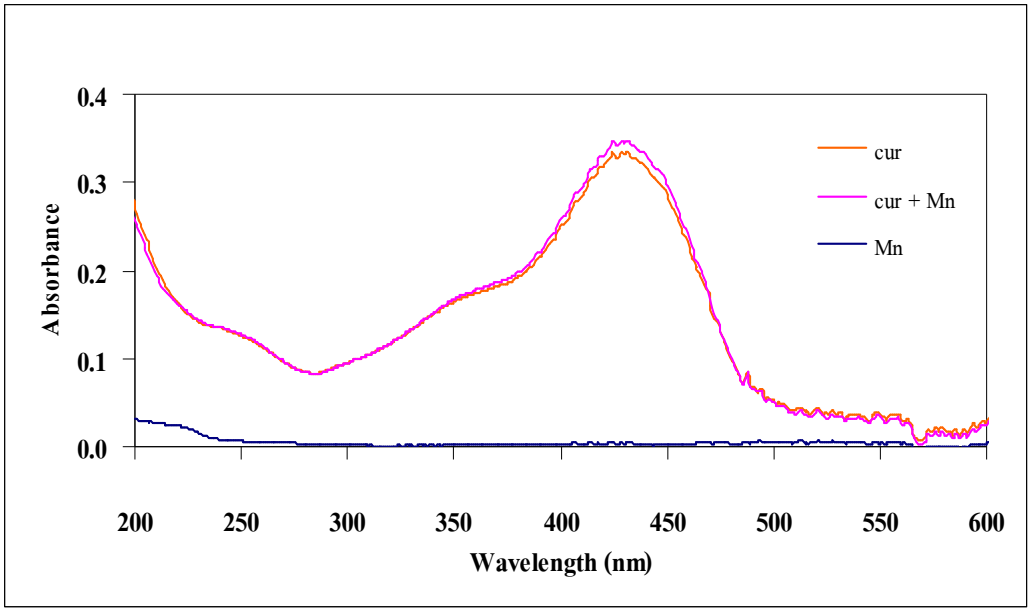

Figure 22 UV-Vis absorption spectra of Mn^{2+}, curcumin and curcumin-Mn^{2+}

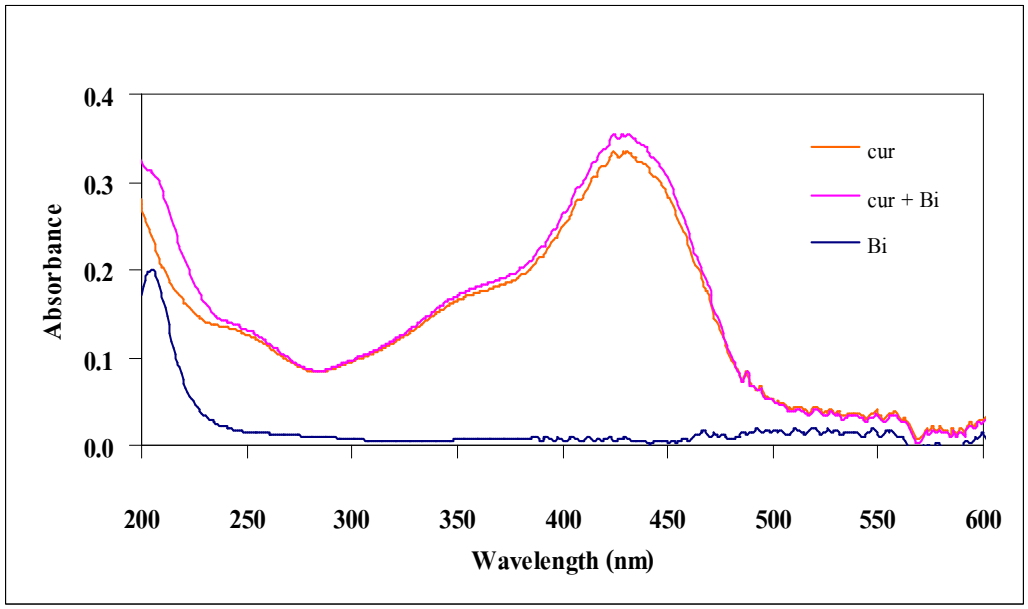

Figure 23 UV-Vis absorption spectra of Bi^{2+}, curcumin and curcumin-Bi^{2+}

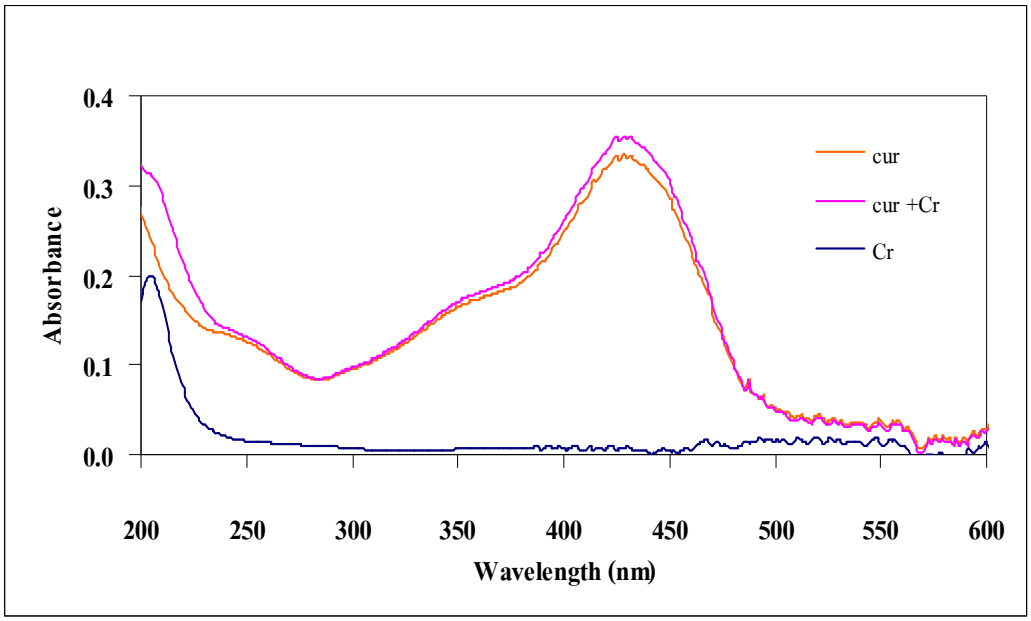

Figure 24 UV-Vis absorption spectra of Cr^{3+}, curcumin and curcumin-Cr^{3+}

3.2 Cyclic voltammetry

3.2.1 Electrochemical behavior of the curcumin

The cyclic voltammograms of curcumin were obtained in an aqueous system at pH 10.30 and 3.65. In order to adjust such value to the experimental requirements, HCl was added to the solutions accordingly. Figure 25 displays the cyclic voltammograms of curcumin (1×10^{-3} M) at pH 10.30 on GCE with the potential scan in the cathodic direction. Figure 26 shows the voltammogram with the potential scan started in the anodic direction which revealed that there were no reduction and oxidation processes in both scan directions.

The voltammogram in Figure 27 started in cathodic direction and Figure 28 started in anodic direction for curcumin [1x10^{-3} M] at pH 3.3 on GCE. There were no peak in both processes. Cyclic voltammograms of curcumin in basic medium and acid medium, on CPE were shown in Figure 29 to Figure 32. Both in Figure 29 and 31 the first scan was in cathodic direction and Figures 30 and 32 were started scanning in the anodic direction. In basic medium, the oxidation peak occurred at potential of 0.40 V. During reverse scans no reaction of reduction were detected. In acid medium, the results are similar to those obtained from using GCE.

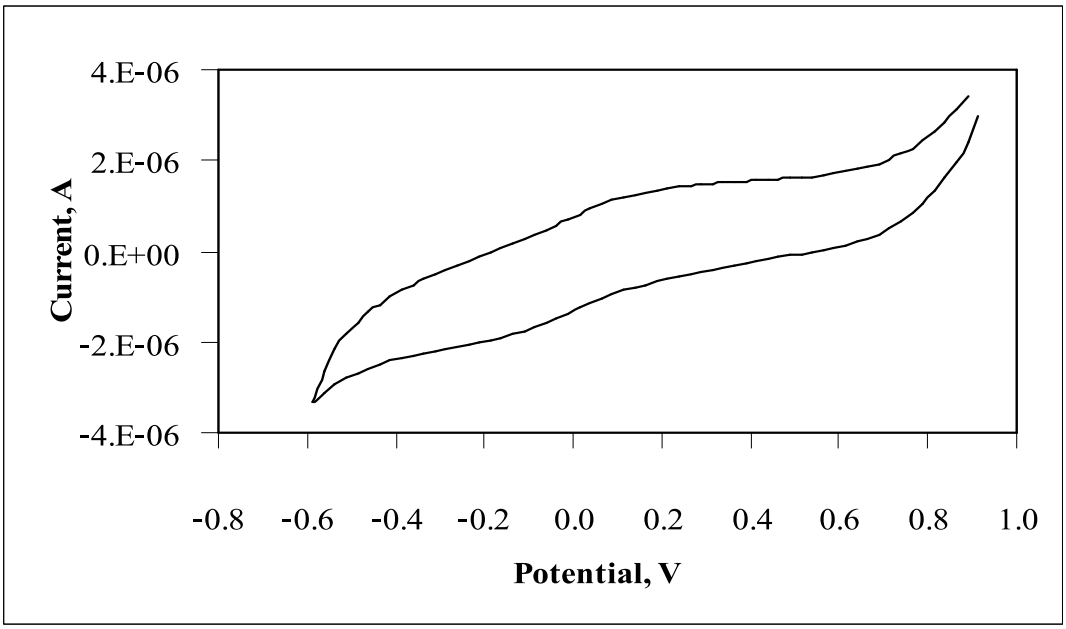

Figure 25 Cyclic voltammogram of the curcumin (1 × 10^{-3} M) in basic medium; pH 10.30 at GCE, at a scan rate of 100 mV/s (cathodic direction)

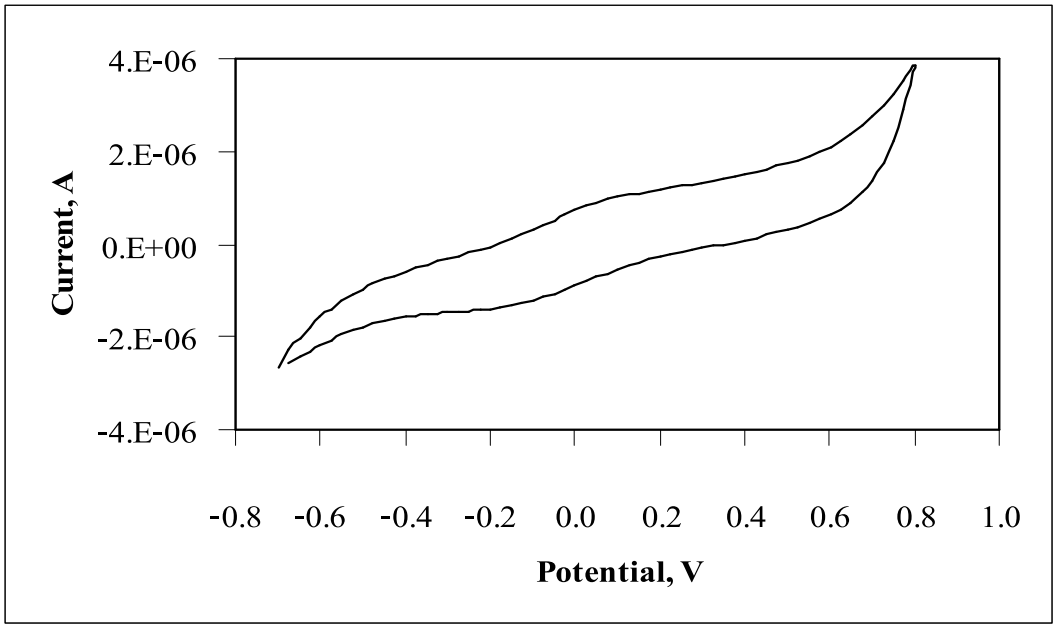

Figure 26 Cyclic voltammogram of the curcumin (1×10^{-3} M) in basic medium; pH 10.30 at GCE, at a scan rate of 100 mV/s (anodic direction)

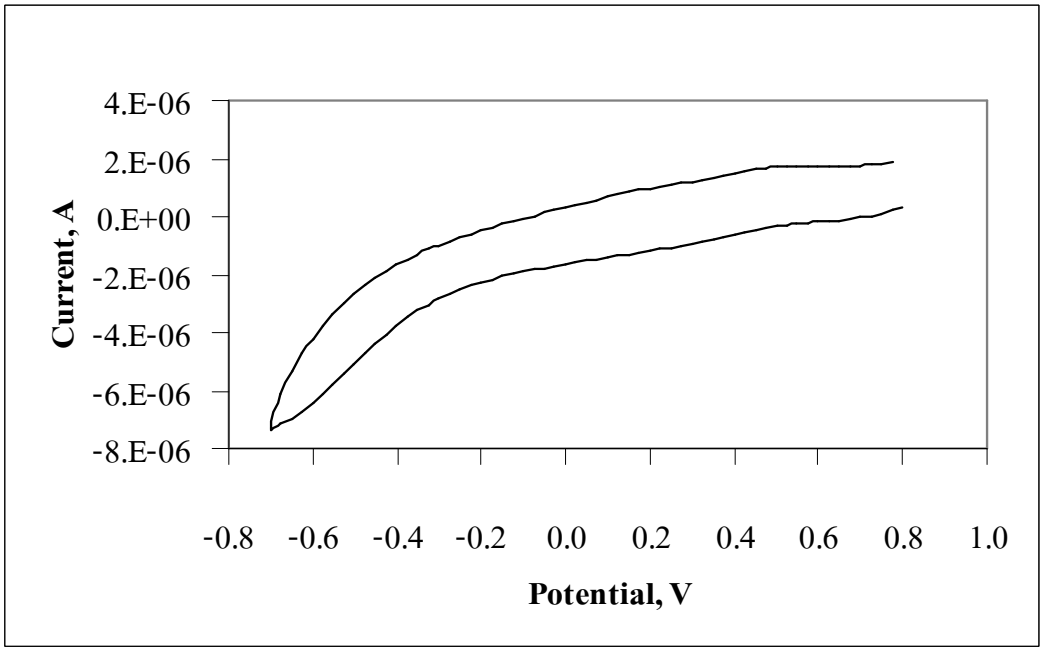

Figure 27 Cyclic voltammogram of the curcumin (1×10^{-3} M) in acid medium; pH 3.3 at GCE, at a scan rate of 100 mV/s (cathodic direction)

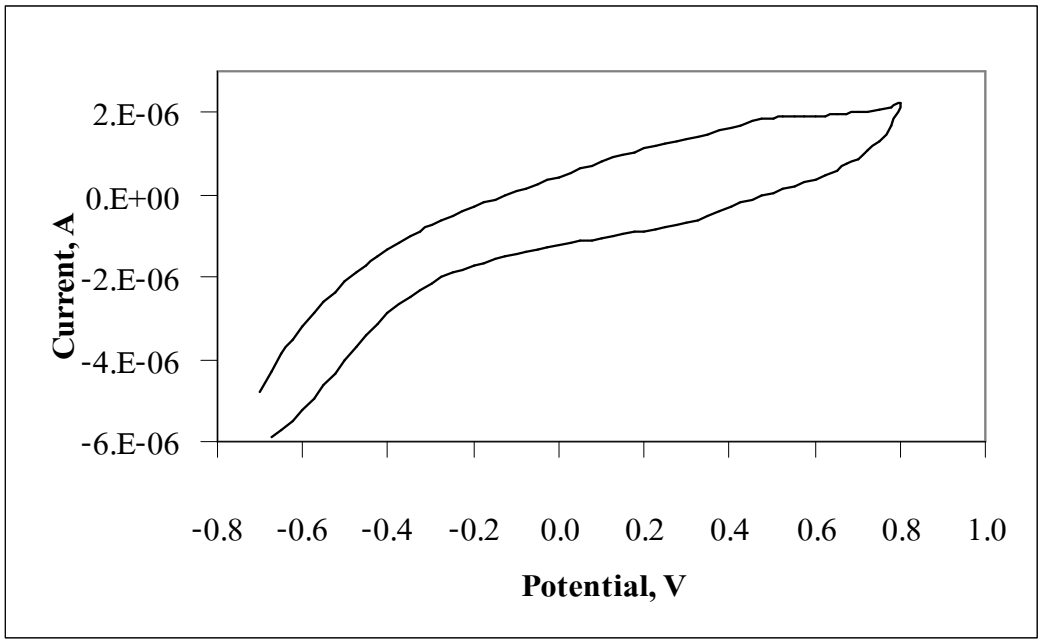

Figure 28 Cyclic voltammogram of the curcumin (1×10^{-3} M) in acid medium; pH 3.3 at GCE, at a scan rate of 100 mV/s (anodic direction)

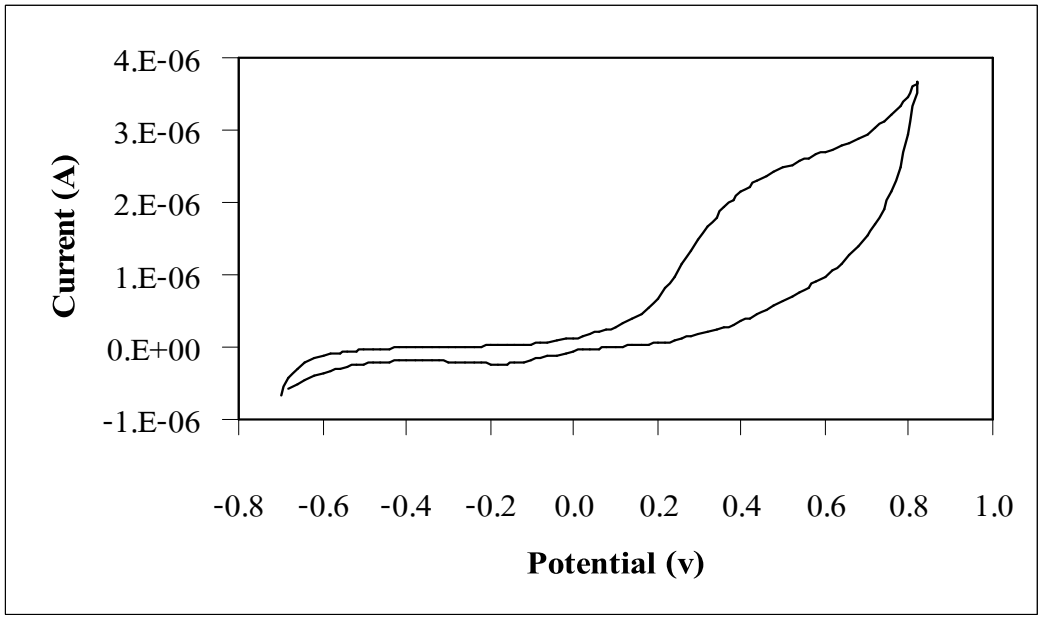

Figure 29 Cyclic voltammogram of the curcumin (1×10^{-3} M) in basic medium; pH 10.77 at CPE, at a scan rate of 100mV/s (cathodic direction)

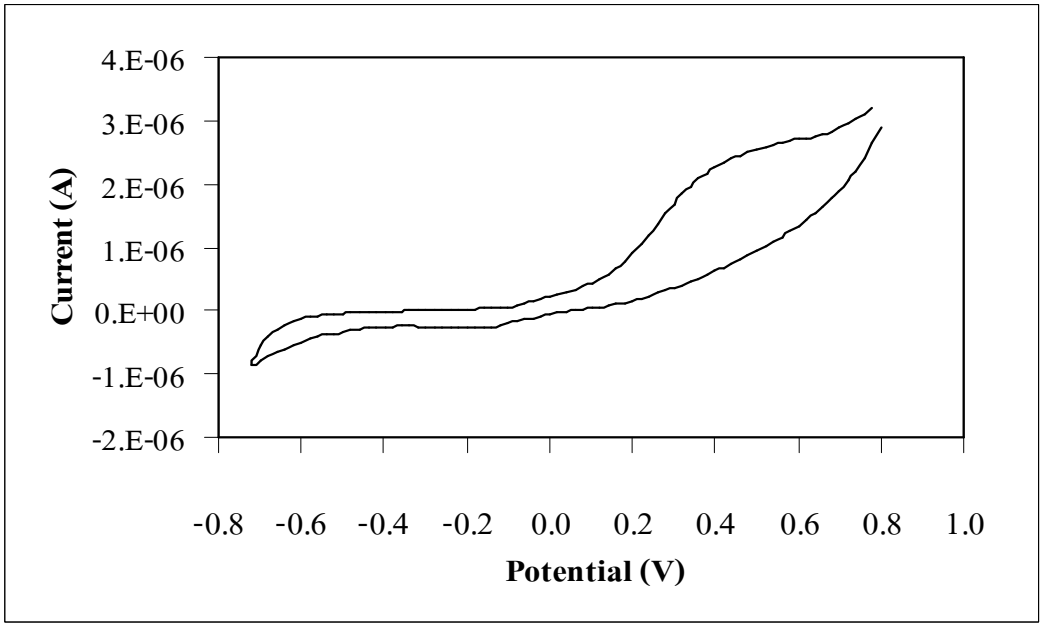

Figure 30 Cyclic voltammogram of the curcumin (1×10^{-3} M) in basic medium; pH 10.77 at CPE, at a scan rate of 100mV/s (anodic direction)

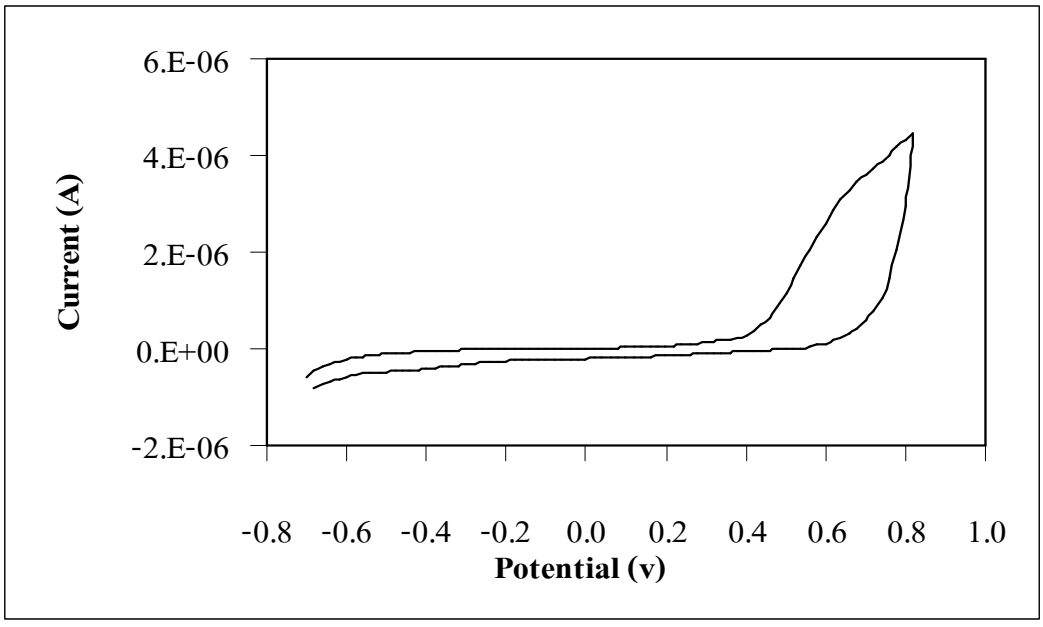

Figure 31 Cyclic voltammogram of the curcumin (1×10^{-3} M) in acid medium; pH 3.65 at CPE, at a scan rate of 100 mV/s (cathodic direction)

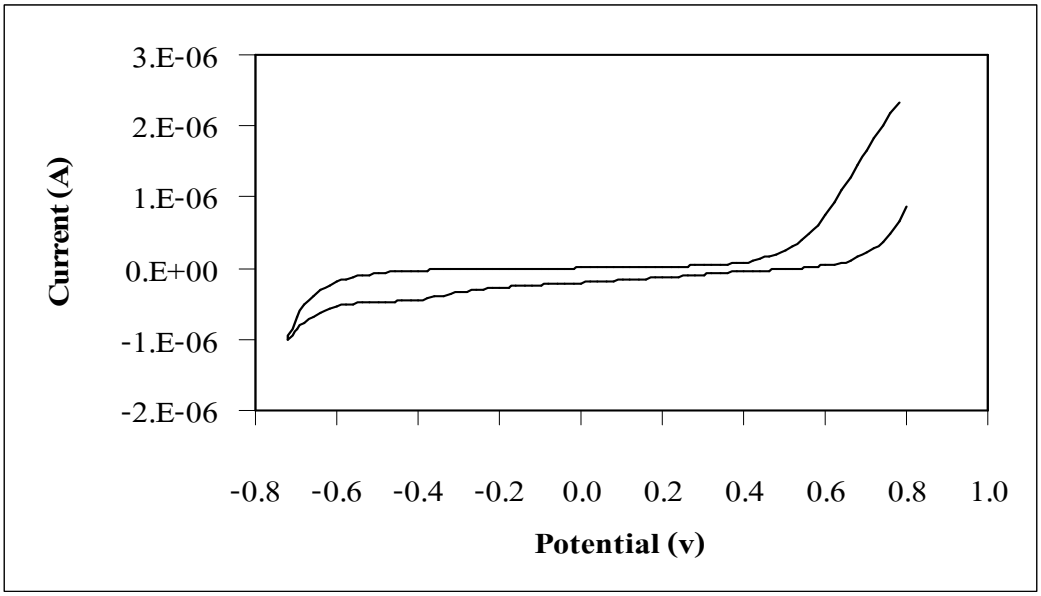

Figure 32 Cyclic voltammograms of the curcumin (1×10^{-3} M) in acid medium; pH 3.65 at CPE, at a scan rate of 100 mV/s (anodic direction)

3.2.2 Electrochemical behavior of the metal ions (Pb^{2+}, Fe^{2+}, Mn^{2+}, Ni^{2+}, Cu^{2+}, As^{5+}, Hg^{2+} and Cr^{2+}).

Cyclic voltammograms of all blank solutions were recorded in the potential window of 0.5 V to -1.25 V vs Ag/AgCl. No significant peak were obtained, indicating that there were no significant impurities as shown in Figure 33.

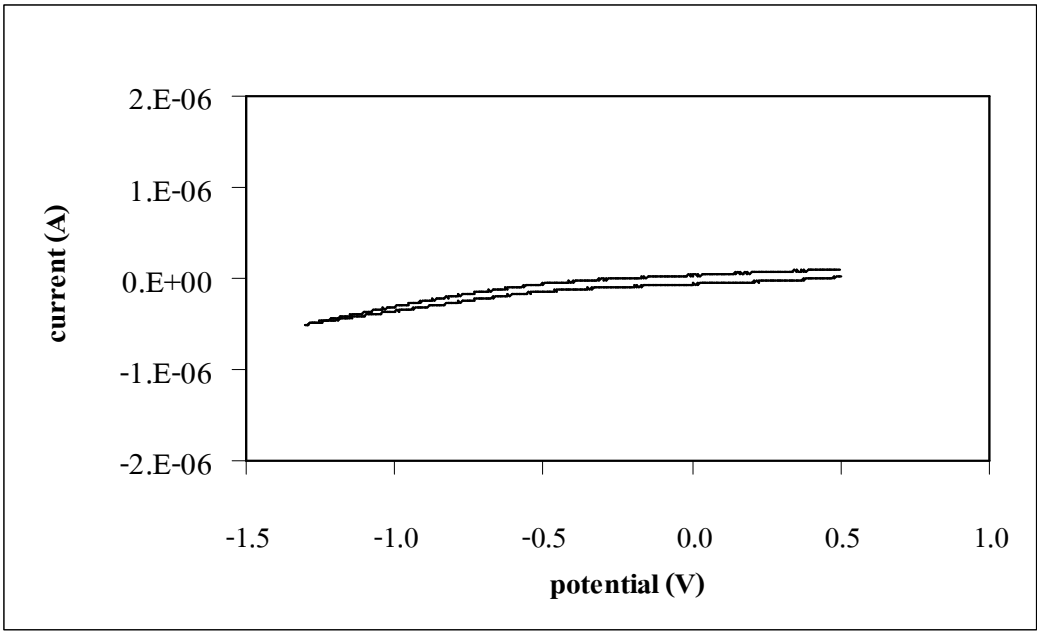

Figure 33 Cyclic voltammogram of ammonium acetate buffer at scan rate 100 mV/s

Cyclic voltammetric data of Pb^{2+}, Hg^{2+} and Cu^{2+} ions were shown in Table 5. For Fe^{2+}, Mn^{2+}, Ni^{2+}, As^{5+} and Cr^{2+} no peak was observed because metal ions are inactive in this condition.

Table 5 Cyclic voltammetric data of Pb^{2+}, Hg^{2+} and Cu^{2+} ions in ammonium acetate buffer at scan rate 100 mV/s

Metals	$E_{1/2}$ (V)	
	Oxidation	Reduction
Pb^{2+}	-0.51	-0.62
Hg^{2+}	0.40	-
Cu^{2+}	0.12	-

The cyclic voltammogram of Hg^{2+} and Cu^{2+} obtains only oxidation peaks at 0.40 V and 0.02 V vs Ag/AgCl, respectively. For Pb^{2+}, eventhough one oxidation and reduction peak were observed at -0.51 V and -0.62 V vs Ag/AgCl, respectively, it still behaves electrochemical irreversible. The voltammograms are shown in Figure 34 to Figure 36.

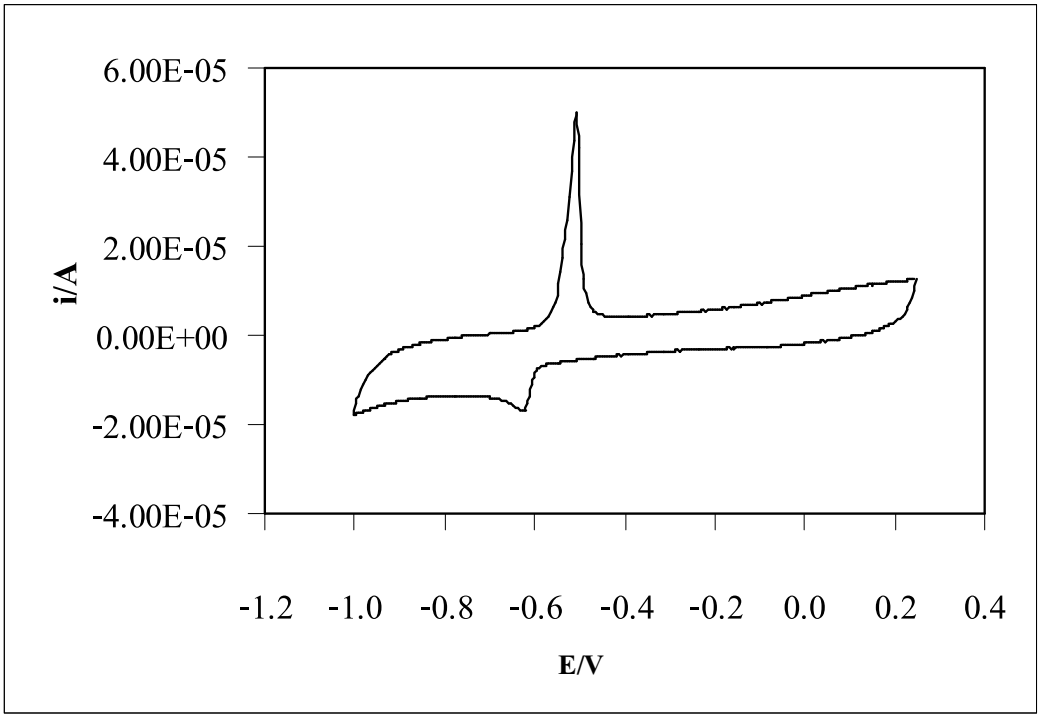

Figure 34 Cyclic voltammogram of 1 x 10^{-4} M Pb^{2+} at GCE in ammonium acetate buffer at scan rate 100 mV/s

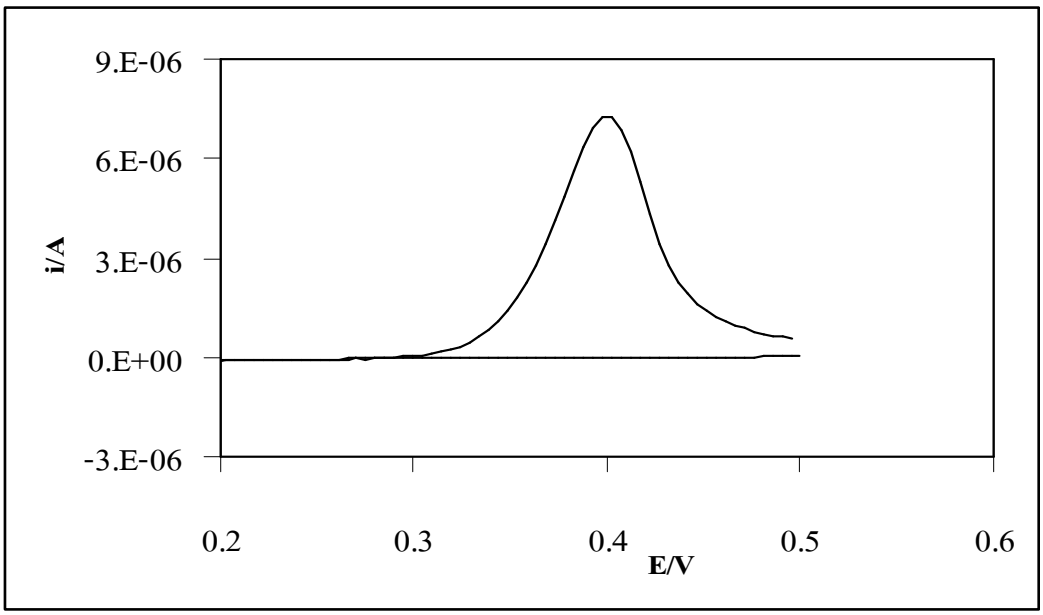

Figure 35 Cyclic voltammogram of 1 x 10^{-4} M Hg^{2+} at GCE in ammonium acetate buffer at scan rate 100 mV/s

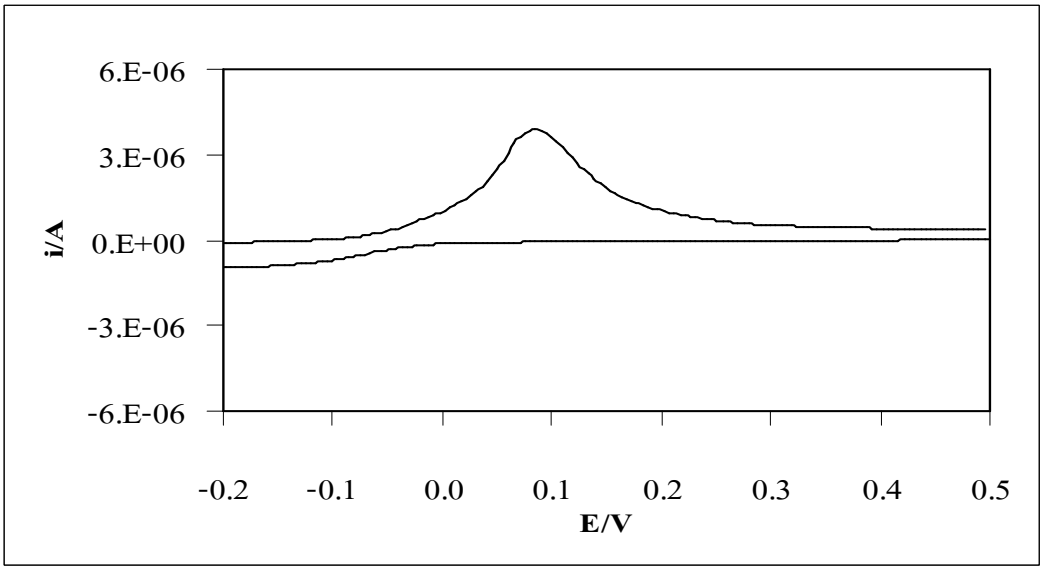

Figure 36 Cyclic voltammogram of 1 x 10^{-4} M Cu^{2+} at GCE in ammonium acetate buffer at scan rate 100 mV/s

3.2.3 Study of complex between Ni^{2+} and curcumin by CV (pH 10)

The stoichiometry of the formed complexes were determined on the basis of the dependence between Ni^{2+} reduction peak current and ligand to metal molar concentration ratio. Figure 37 shows cyclic voltammogram of the Ni^{2+}-curcumin system was measured at pH 10. This system was run at scan rate 100 mV/s. The oxidation peak occured at 0.15 V vs Ag/AgCl and when the scan was reversed the reduction peak appeared at -0.15 V vs Ag/AgCl.

The plots of peak current (i_p) dependence on the solution composition are shown in Figure 38. It can be seen that the current versus molar ratio plot does not give a sharp break, as usual indication of complex formation. Therefore, the complexation of Ni^{2+} with curcumin did not take place. Data of these plots are shown in Table 6.

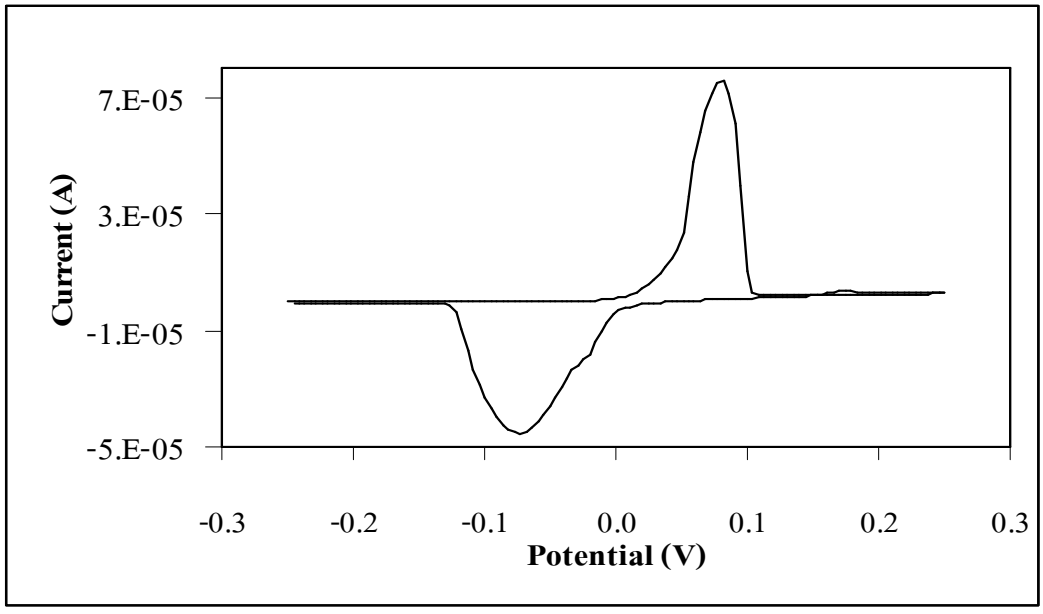

Figure 37 Cyclic voltammogram of Ni^{2+}-curcumin system at HMDE in ammonium acetate buffer at scan rate 100 mV/s

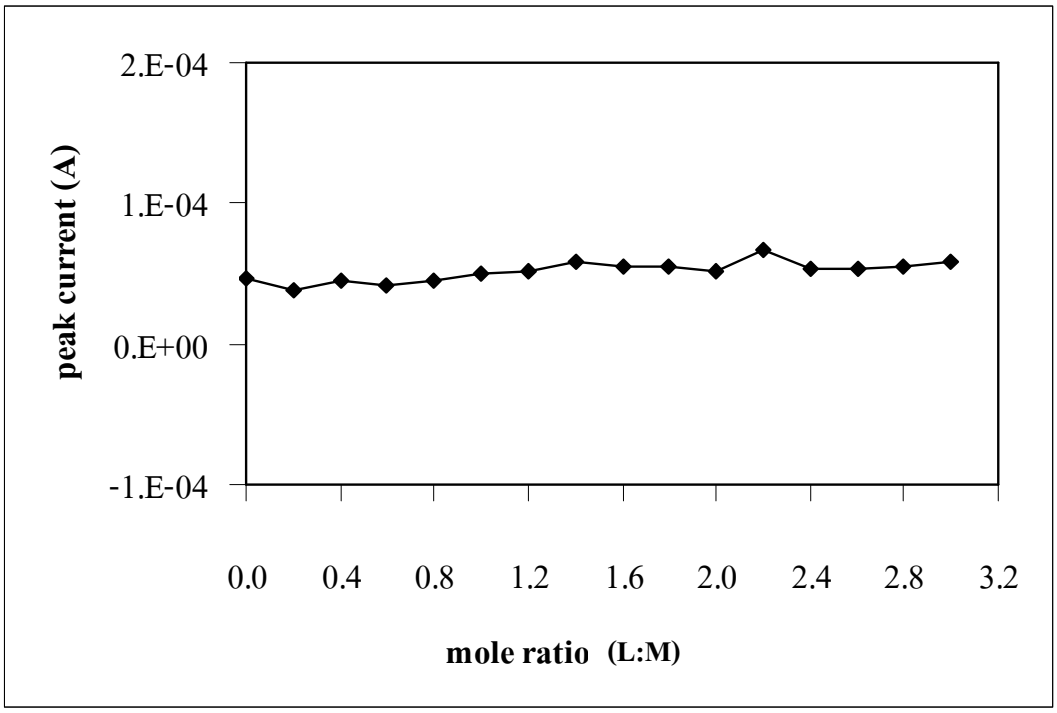

Figure 38 Plots of i_p versus ligand to metal molar ratio for Ni^{2+}-curcumin system at scan rate 100 mV/s

3.2.4 Study of complexes between Cd^{2+}, Pb^{2+} and curcumin by CV

The stoichiometries of the complexes were determined on the basis of the dependence between Pb^{2+} (or Cd^{2+}) reduction peak currents and ligand to metal molar concentration ratios. Figure 39 shows cyclic voltammograms for the Pb^{2+}-curcumin system measured at pH 4. This system was run at scan rate 100 mV/s. The anodic peak appeared at -0.383 V and the cathodic peak at -0.338 V which were interpreted as irreversible process. For the Cd^{2+}-curcumin system, at scan rate 100 mV/s, there was the reduction peak at -0.589 V and when the scan was reversed, the oxidation peak appeared at -0.545 V as shown in Figure 40. Both system associated with electrochemical irreversible because the ΔE for both systems was greater than 0.059.

Similar plots for Pb^{2+}-curcumin and Cd^{2+}-curcumin system are shown in Figure 41 and Figure 42. It can be seen that the current versus molar ratio of Cd^{2+} and curcumin plot does not give a sharp break. In this condition curcumin does not form complex with Cd^{2+}. Data of plots for Pb^{2+}-curcumin and Cd^{2+}-curcumin system are shown in Table 6.

However, when GCE was used as working electrode for Pb^{2+}-curcumin system, the current versus molar ratio plot gave a sharp break at 0.8 as shown in Figure 42. This is an indication of complex formation between curcumin and Pb^{2+} in the ratio of 1:1. Data of these plots are shown in Table 7.

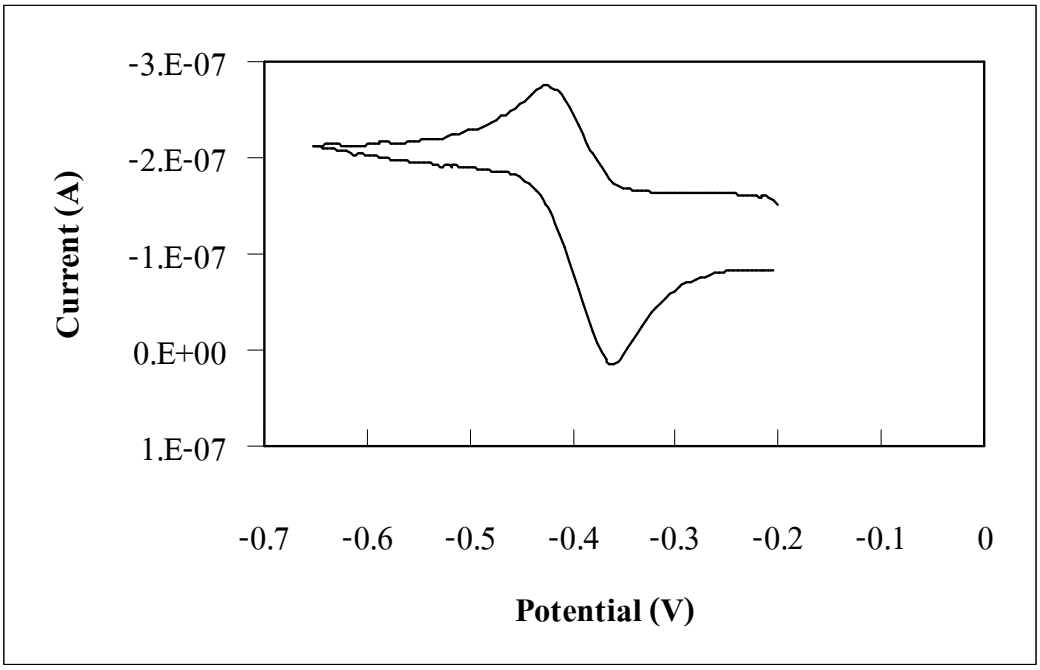

Figure 39 Cyclic voltammogram of Pb^{2+}-curcumin system at HMDE, at scan rate 100 mV/s

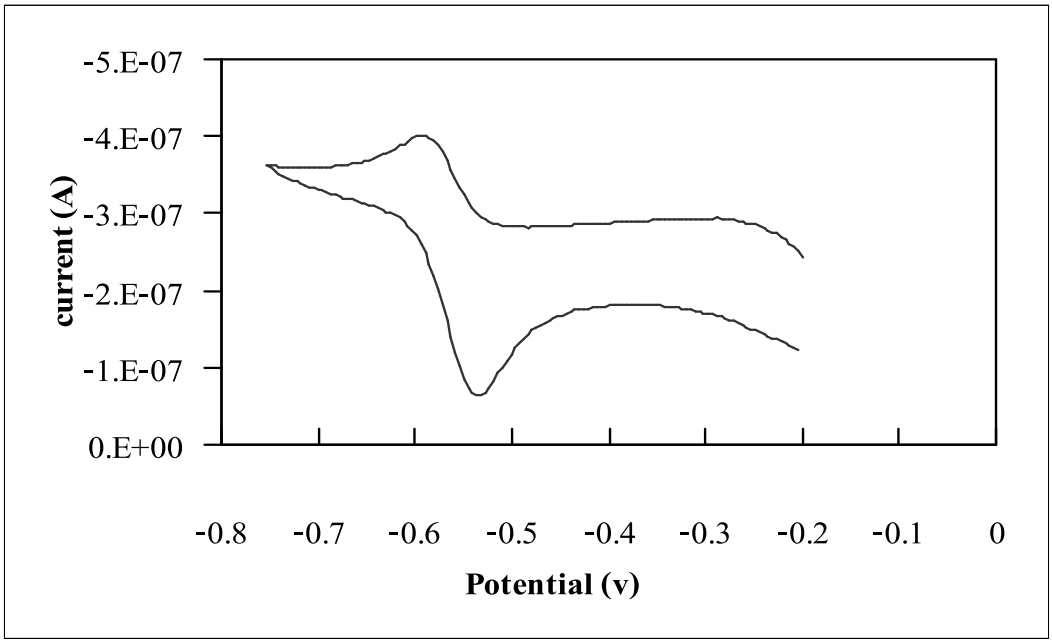

Figure 40 Cyclic voltammogram of Cd^{2+}-curcumin system at HMDE, at scan rate 100 mV/s

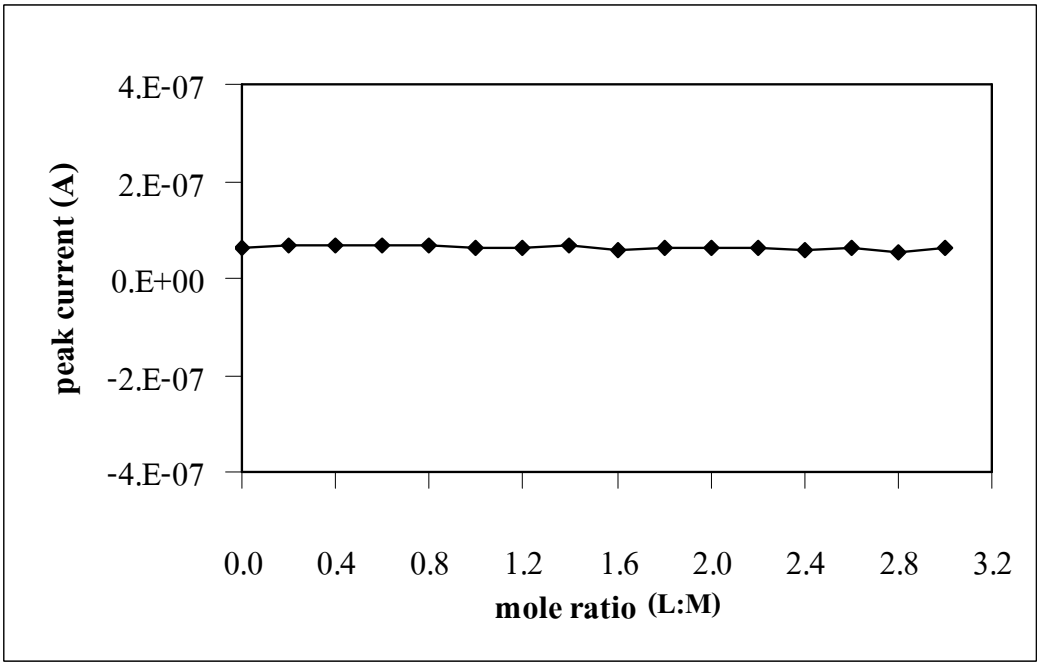

Figure 41 Plots of i_p versus ligand to metal molar ratio for Pb^{2+}-curcumin system at scan rate 100 mV/s

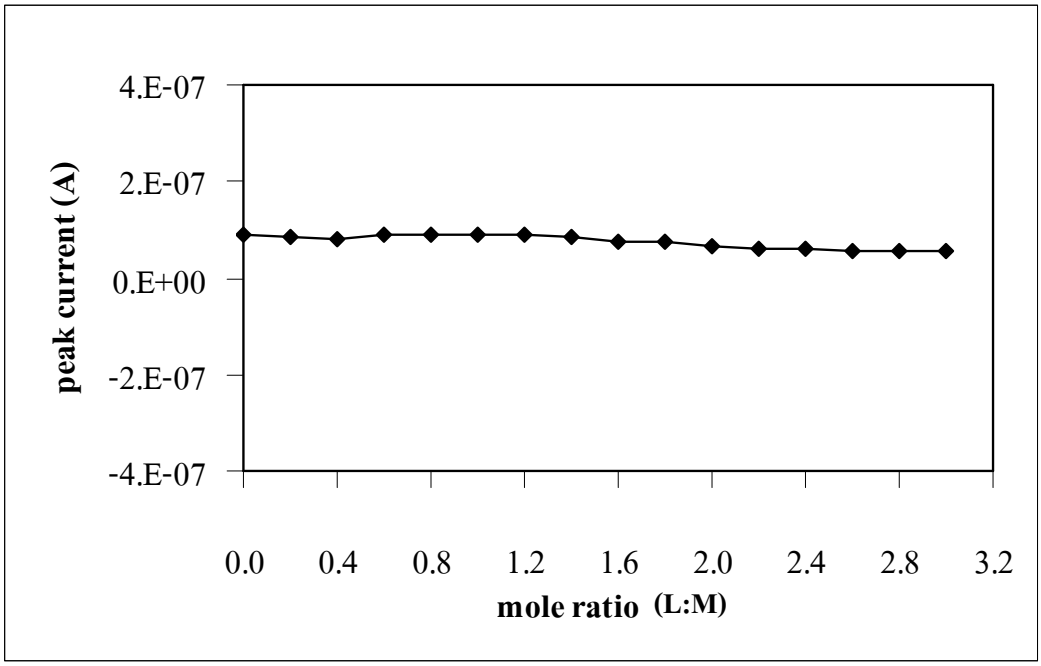

Figure 42 Plots of i_p versus ligand to metal molar ratio for Cd^{2+}-curcumin system at scan rate 100 mV/s

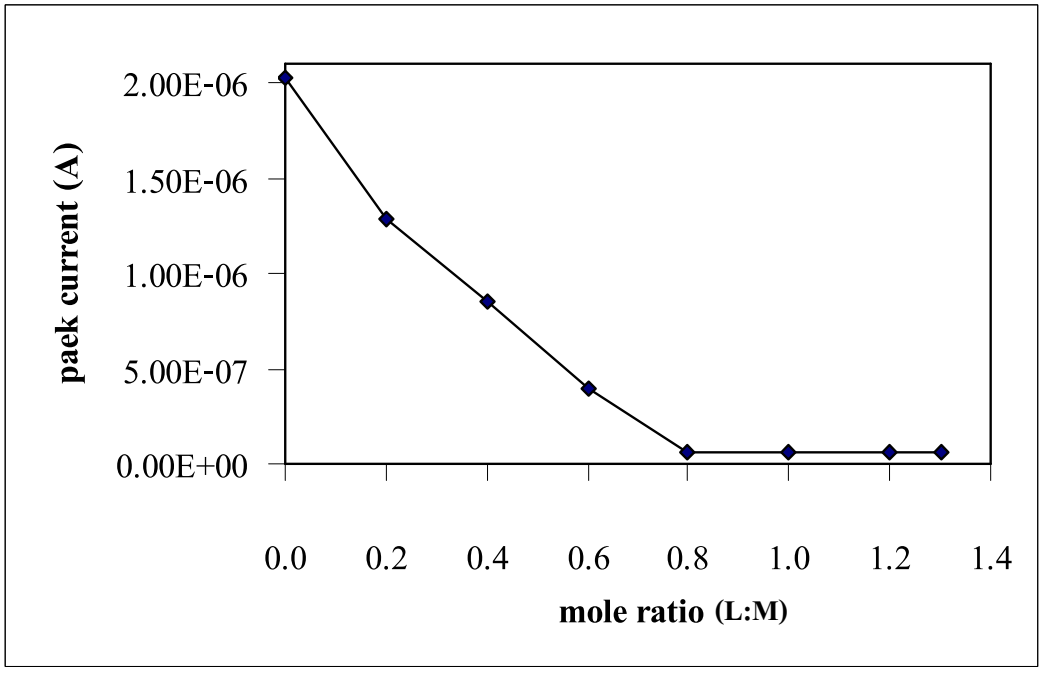

Figure 43 Plots of i_p versus ligand to metal molar ratio for Pb^{2+}-curcumin system at scan rate 100 mV/s

Table 6 Peak current of Pb^{2+}-curcumin, Cd^{2+}-curcumin, and Ni^{2+}-curcumin systems

mole ratio	current Pb^{2+}	S	current Cd^{2+}	S	current Ni^{2+}	S
0.0	6.64E-08	3.81E-09	9.14E-08	7.36E-10	6.64E-08	3.81E-09
0.2	6.64E-08	3.81E-09	8.51E-08	1.25E-09	6.64E-08	3.81E-09
0.4	6.54E-08	2.05E-09	8.11E-08	5.89E-10	6.54E-08	2.05E-09
0.6	6.61E-08	1.25E-09	9.06E-08	6.24E-10	6.61E-08	1.25E-09
0.8	6.75E-08	2.16E-09	9.10E-08	5.56E-10	6.75E-08	2.16E-09
1.0	6.33E-08	2.45E-09	8.89E-08	8.98E-10	6.33E-08	2.45E-09
1.2	6.30E-08	2.05E-09	8.93E-08	8.16E-10	6.30E-08	2.05E-09
1.4	6.79E-08	1.63E-09	8.40E-08	8.16E-10	6.79E-08	1.63E-09
1.6	6.01E-08	1.63E-09	7.60E-08	2.45E-09	6.01E-08	1.63E-09
1.8	6.37E-08	4.19E-09	7.38E-08	8.22E-10	6.37E-08	4.19E-09
2.0	6.31E-08	2.05E-09	6.64E-08	1.63E-09	6.31E-08	2.05E-09
2.2	6.27E-08	1.70E-09	6.17E-08	8.16E-10	6.27E-08	1.70E-09
2.4	5.93E-08	6.60E-10	6.18E-08	8.16E-10	5.93E-08	6.60E-10
2.6	6.11E-08	4.08E-10	5.34E-08	8.16E-10	6.11E-08	4.08E-10
2.8	5.28E-08	1.25E-10	5.42E-08	1.63E-09	5.28E-08	1.25E-10
3.0	6.16E-08	4.97E-10	5.38E-08	1.63E-09	6.16E-08	4.97E-10

Table 7 Peak current of Pb^{2+}-curcumin system

mole ratio	current (Pb^{2+})	S
0.0	2.56E-06	6.11E-07
0.2	1.43E-06	1.41E-07
0.4	8.37E-07	4.16E-08
0.6	3.67E-07	2.65E-08
0.8	5.53E-08	2.18E-09
1.0	5.60E-08	1.74E-09
2.0	5.56E-08	1.58E-09
3.0	5.55E-08	2.14E-09

3.3 Nuclear magnetic resonance spectroscopy

Nuclear magnetic resonance spectroscopy of curcumin is a technique to determine the molecular structure of a compound. The structure of ligand and complexes were investigated by using ^{1}H and ^{13}C NMR. The NMR spectra of all compounds were recorded in $CDCl_3$ and d_6-DMSO. The tetramethylsilane ($Si(CH_3)_4$) was used as an internal reference.

3.3.1 NMR spectroscopy of curcumin

Table 8 ^{1}H NMR spectroscopic data of curcumin ($CDCl_3$)

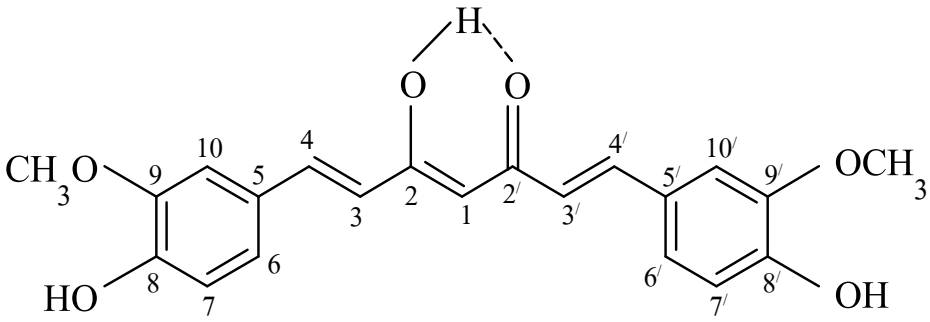

H-position	^{1}H NMR		
	δ(ppm)	J (Hz)	Number of H
1	5.8 (s)	-	1
2-OH	16.1 (bs)	-	1
3,3′	6.5 (d)	15.6	2
4,4′	7.6 (s)	15.6	2
5,5′	-	-	-
6,6′	7.1 (dd)	8.4	2
7,7′	6.9 (d)	8.4	2
8,8′-OH	-	-	2
9,9′	-	-	-
10,10′	7.3 (s)	-	2
OMe	3.9 (s)	-	6

s = singlet, bs = broad singlet, d = doublet, dd = doublet of doublet

The structure and the related NMR data are shown in Table 8. The H-1 signal at 5.8 ppm in the NMR spectrum of curcumin indicates the presence of the methine proton in the enolic form. The olefinic protons H-4 and H-4′ adjacent to the aromatic

ring appear downfield as compared to H-3 and H-3′. Among the aromatic protons, H-6 and H-10 resonate at downfield and H-7 upfield. The ^{1}H NMR spectra of curcumin in $CDCl_3$ and d_6-DMSO are shown in Figure 44 and 45, respectively. In addition, the peak assignments are supported by the correlation ^{1}H-^{1}H COSY NMR spectroscopy. The ^{1}H-^{1}H COSY NMR signals are shown in Figure 46.

Table 9 ^{1}H NMR and ^{13}C NMR spectroscopic data of curcumin (d_6-DMSO)

H-position	^{1}H NMR			^{13}C NMR
	δ(ppm)	J (Hz)	Number of H	δ(ppm)
1	6.1 (s)	-	1	100.9
2-OH	16.1 (bs)	-	1	183.4
3,3′	7.5 (d)	16	2	121.3
4,4′	6.7 (s)	16	2	140.9
5,5′	-	-	-	126.5
6,6′	7.2 (dd)	2, 8.1	2	123.3
7,7′	6.8 (d)	8.1	2	115.9
8,8′-OH	9.6 (s)	-	2	149.5
9,9′	-	-	-	148.3
10,10′	7.3 (s)	-	2	111.5
OCH_3	3.9 (s)	-	6	55.9

^{13}C NMR spectrum of curcumin exhibited twelve signals from 21 carbons consistent with symmetry around C-1 carbons (Table 9). Assignments were made by comparing the observed values with the calculated values obtained by adding incremental shifts for substituents to the base value for a given system. A benzene ring

was considered as the basic system for which the incremental shift due to –OH, –OCH_3 and –CH=CH– were added for calculating the chemical shift values for the aromatic carbons. The two carbonyl carbons, viz. C-2 and C-2/ appeared at 183.4 ppm. The carbon signals at 149.5 and 121.3 ppm were assigned to the C-4 and C-3 (–CH=CH–). The signals at 148.3 and 126.5 ppm was due to quaternary carbon C-9 and C-5 of the phenyl ring. The signals of carbon C-6, C-7, and C-10 appeared at 123.3, 115.9 and 111.6 ppm. The highest field signal could be assigned to the methoxy group. The ^{13}C NMR spectrum of curcumin is shown in Figure 47.

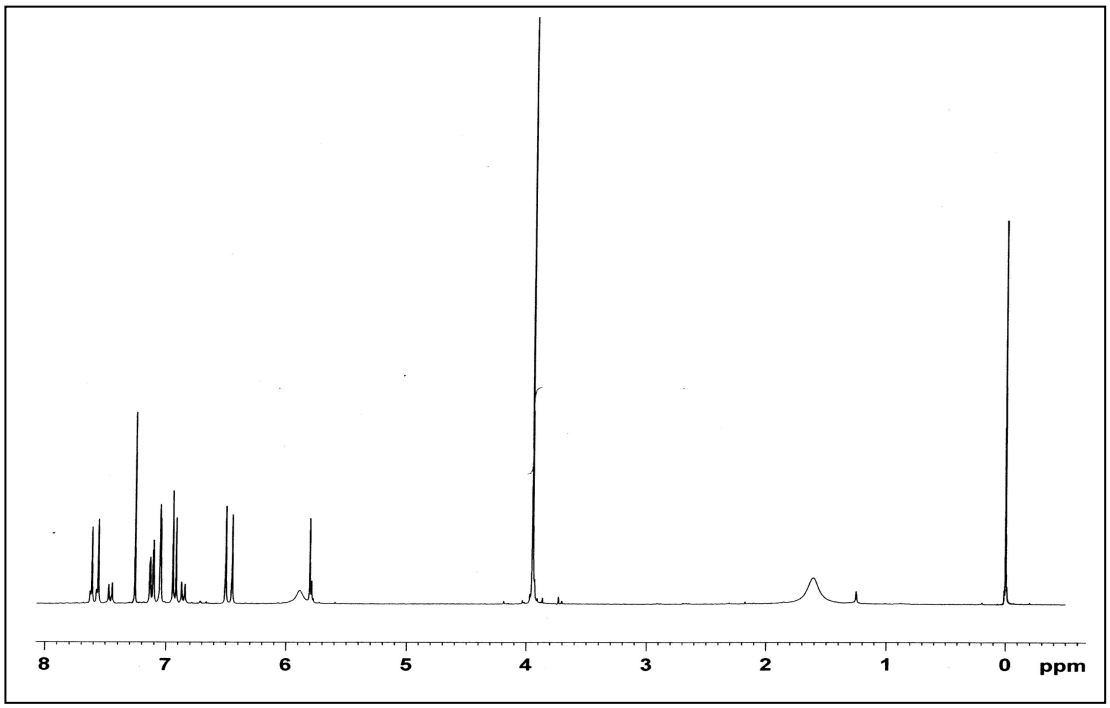

Figure 44 ^{1}H NMR spectrum of curcumin in $CDCl_3$

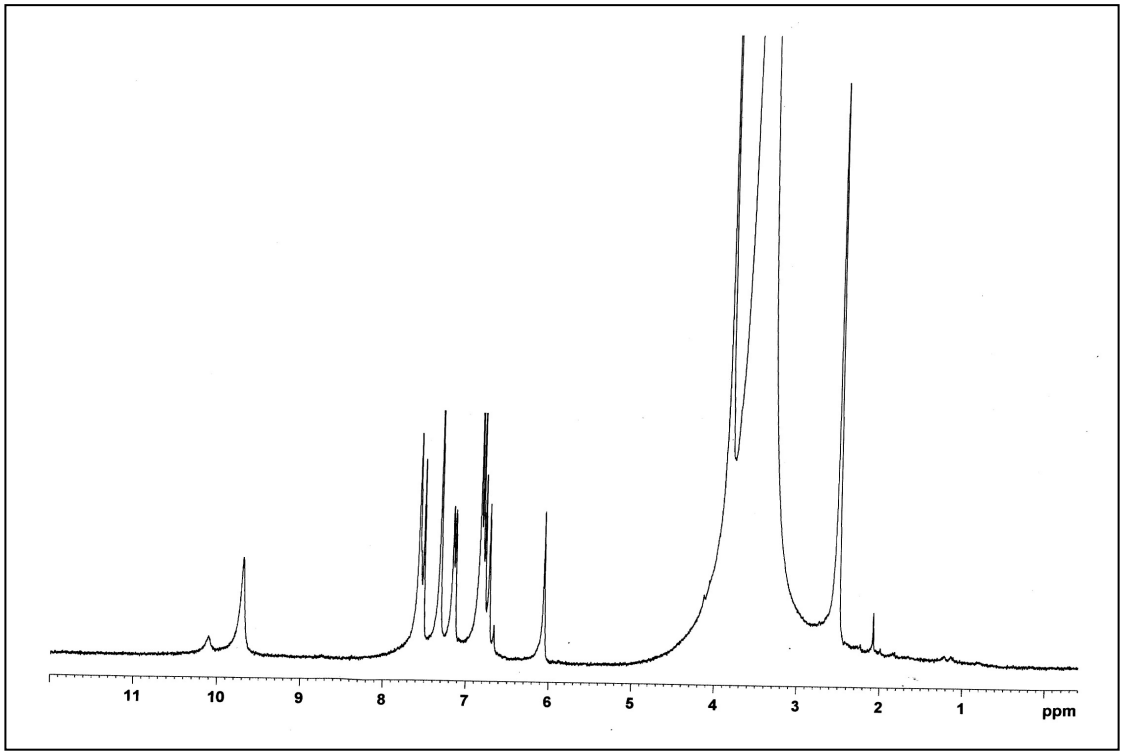

Figure 45 ^{1}H NMR spectrum of curcumin in d_6- DMSO

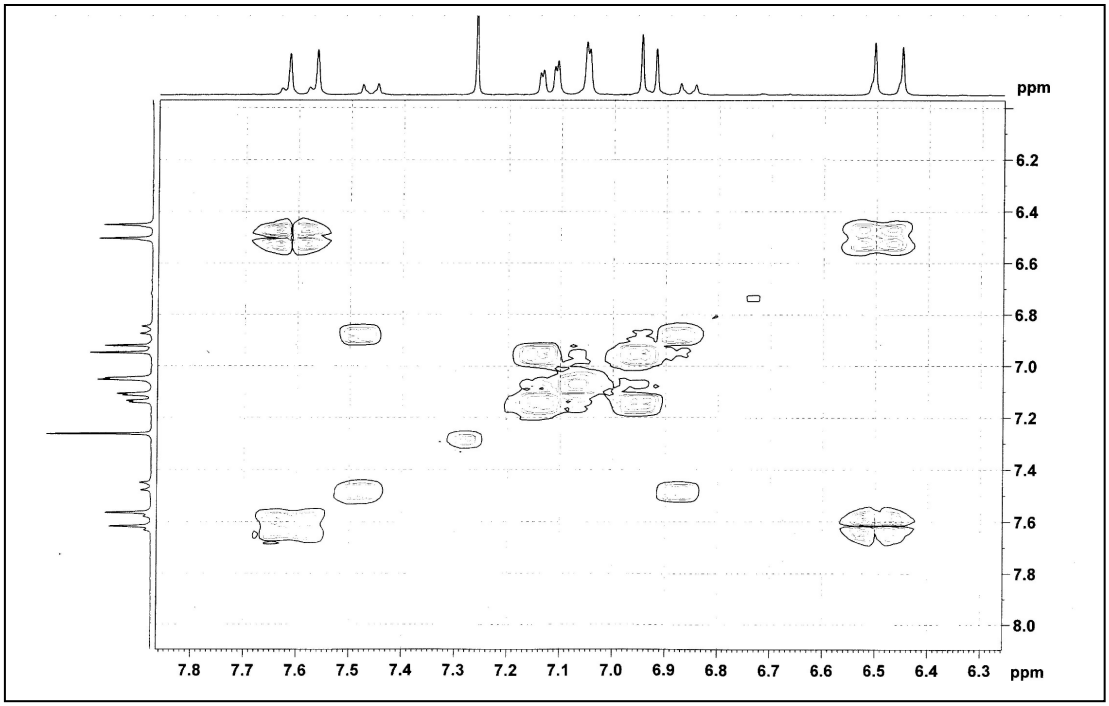

Figure 46 ^{1}H-^{1}H COSY NMR spectrum of curcumin in $CDCl_3$

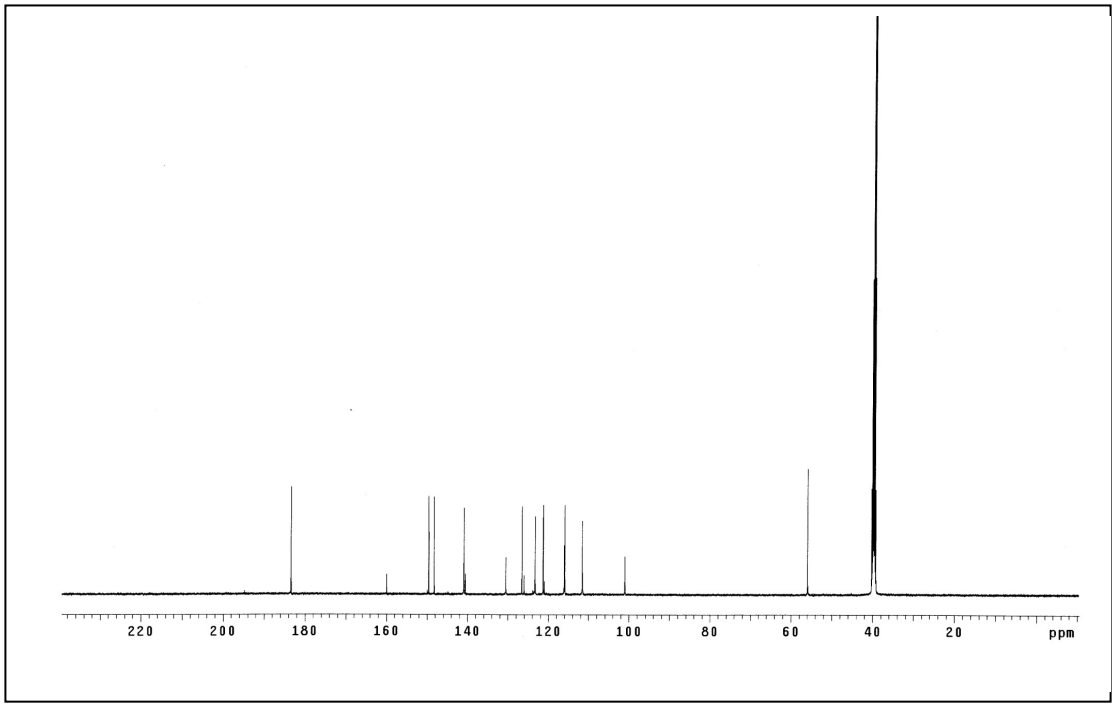

Figure 47 ^{13}C NMR spectrum of curcumin in d_6-DMSO

3.3.2 NMR spectroscopy of curcumin and metal ions

3.3.2.1 ^{1}H NMR study of curcumin and metal ions (Pb^{2+}, Hg^{2+}, Zn^{2+} and Mg^{2+}) in $CDCl_3$

^{1}H NMR data of curcumin-Hg^{2+} and curcumin-Zn^{2+} systems showed a new peak at 5.0 ppm (broad singlet) while the curcumin-Mg^{2+} system at 5.3 ppm. Curcumin-Pb^{2+} system did not show any new peak. The spectra of curcumin-Hg^{2+}, Zn^{2+}, Mg^{2+} and Pb^{2+} are shown in Figure 48 to Figure 51, respectively.

3.3.2.2 ^{1}H NMR study of curcumin and metal ions (Pb^{2+}, Hg^{2+}, Mn^{2+}, Co^{3+}, Cu^{2+}, Zn^{2+} and Mg^{2+}) in d_6-DMSO

In the ^{1}H NMR spectra of curcumin-Pb^{2+} and curcumin-Mg^{2+} (Figure 51 and Figure 53) systems the methine CH proton for the enol form showed highfield shift about 0.4 ppm except curcumin-Zn^{2+} system (Figure 54) which shifted about 0.6 ppm. The other protons did not shift. Spectra of curcumin-Co^{2+}, curcumin-Cu^{2+} and

curcumin-Mn^{2+} systems (Figure 55 to Figure 57) were either broad or featureless. For Curcumin-Cu^{2+} system when adding Cu^{2+} into curcumin solution, the reaction mixture changed color from yellow to red and a solid precipitate was formed. The signals from the aromatic protons, H-6, H-7 and H-10 and the olefinic protons, H-3 and H-4 of curcumin-Hg^{2+} system (Figure 58) appeared very complicate, while the phenolic protons showed broad spectrum in comparison to curcumin.

3.3.2.3 ^{13}C NMR study of curcumin and metal ions (Hg^{2+}, Mn^{2+}) in d_6-DMSO

In the ^{13}C NMR spectrum of curcumin-Mn^{2+} system (Figure 59) all carbons shifted highfield about 7-8 ppm but the curcumin-Hg^{2+} (Figure 60) system did not show any shift.

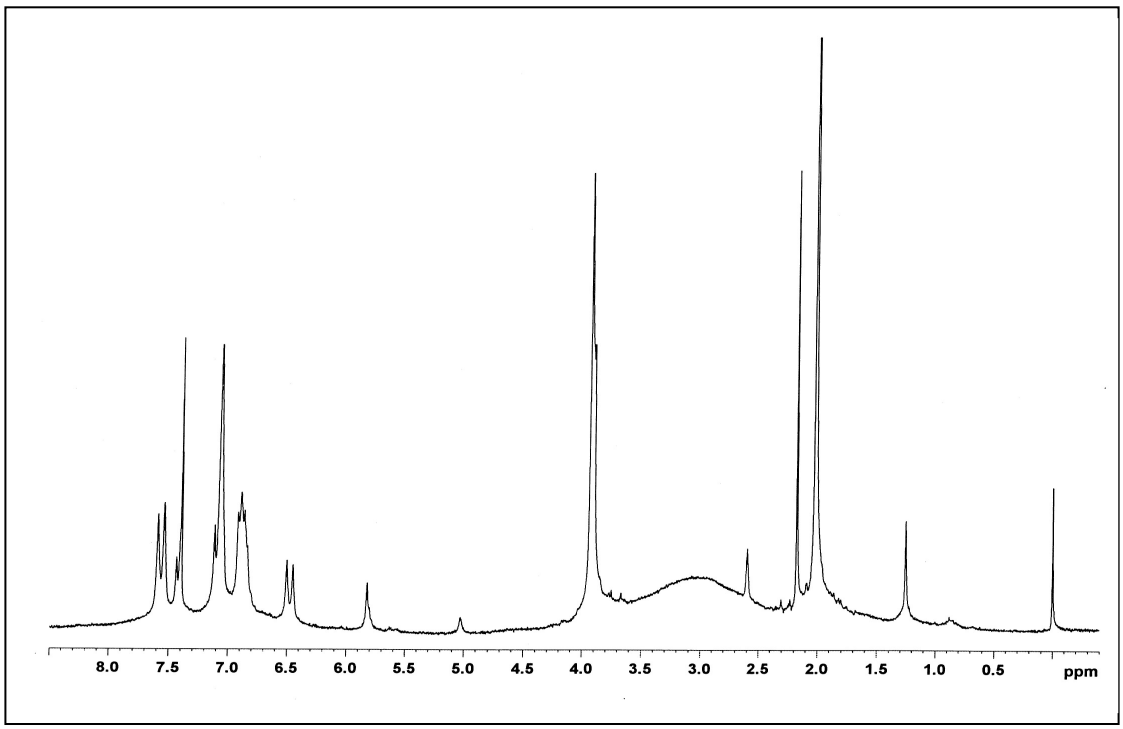

Figure 48 ^{1}H NMR spectrum of curcumin-Hg^{2+} in $CDCl_3$

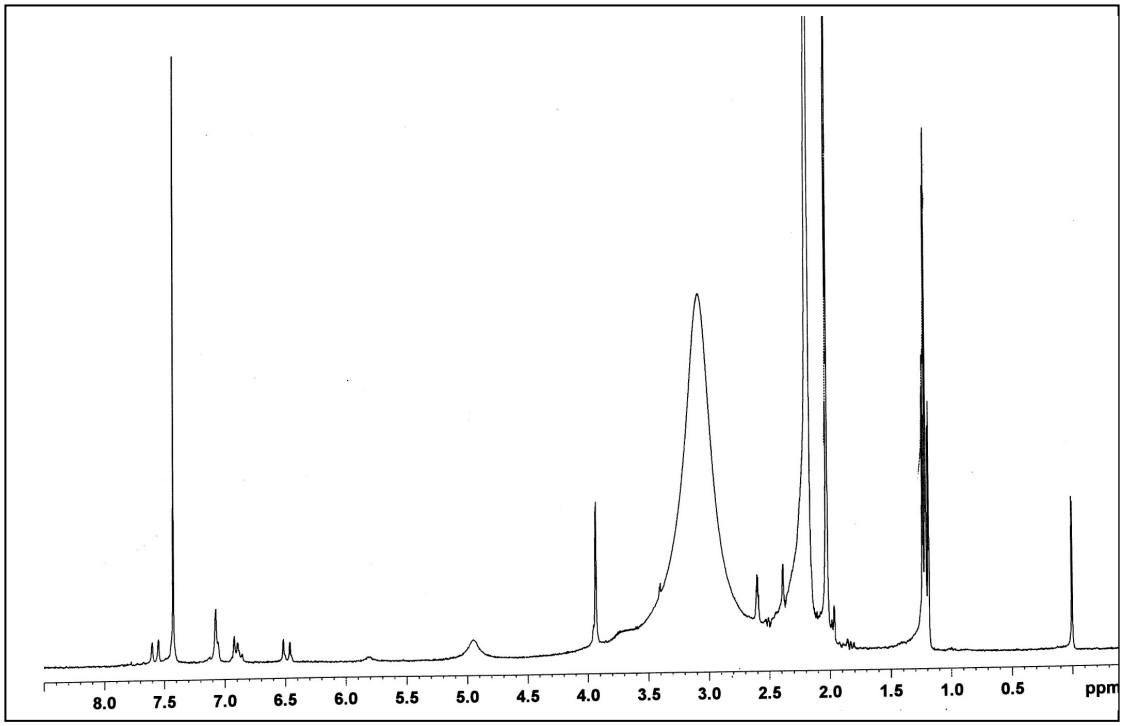

Figure 49 ^{1}H NMR spectrum of curcumin-Zn^{2+} in $CDCl_3$

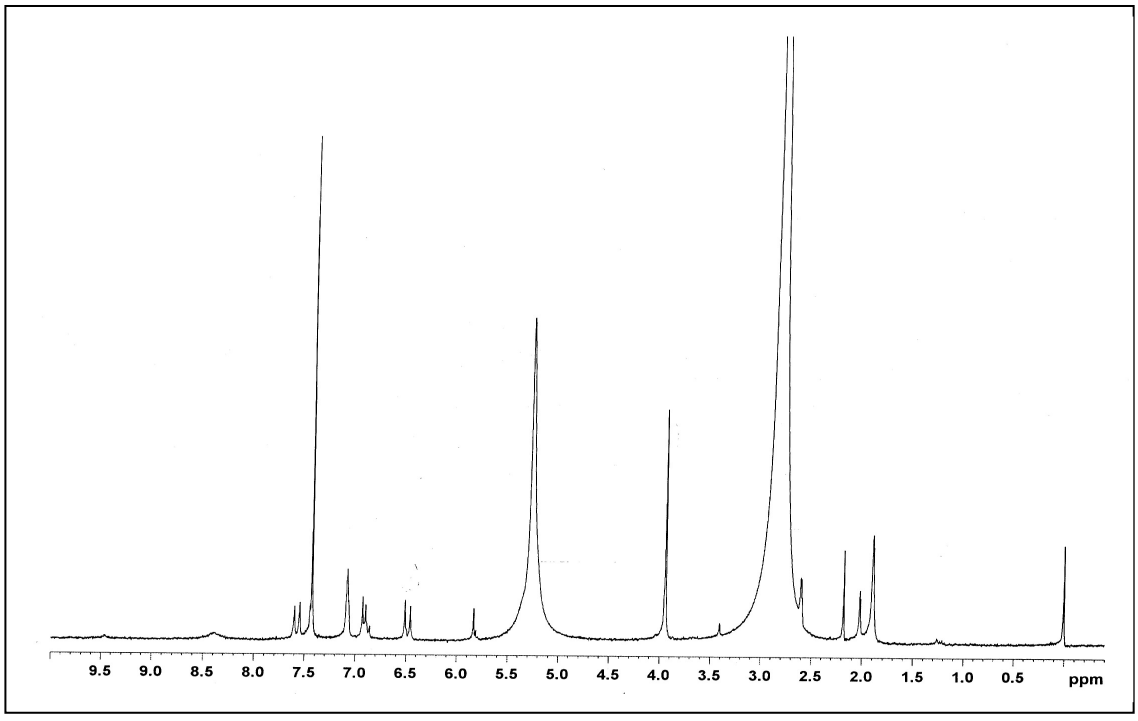

Figure 50 ^{1}H NMR spectrum of curcumin-Mg^{2+} in $CDCl_3$

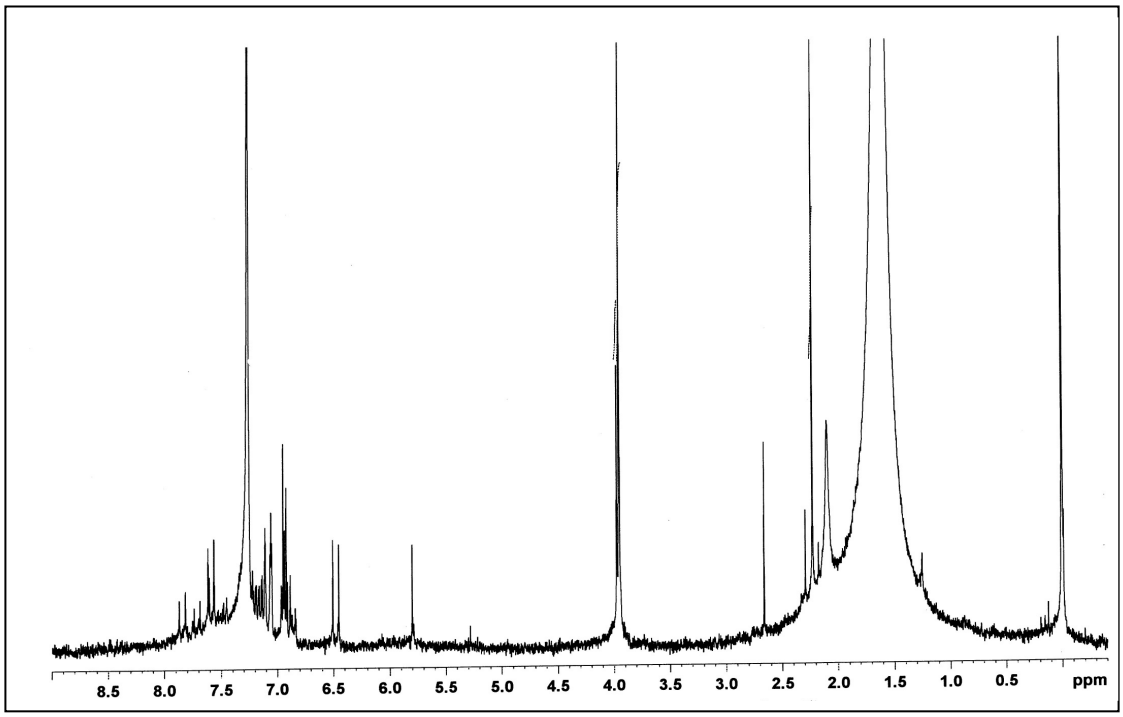

Figure 51 ^{1}H NMR spectrum of curcumin-Pb^{2+} in $CDCl_3$

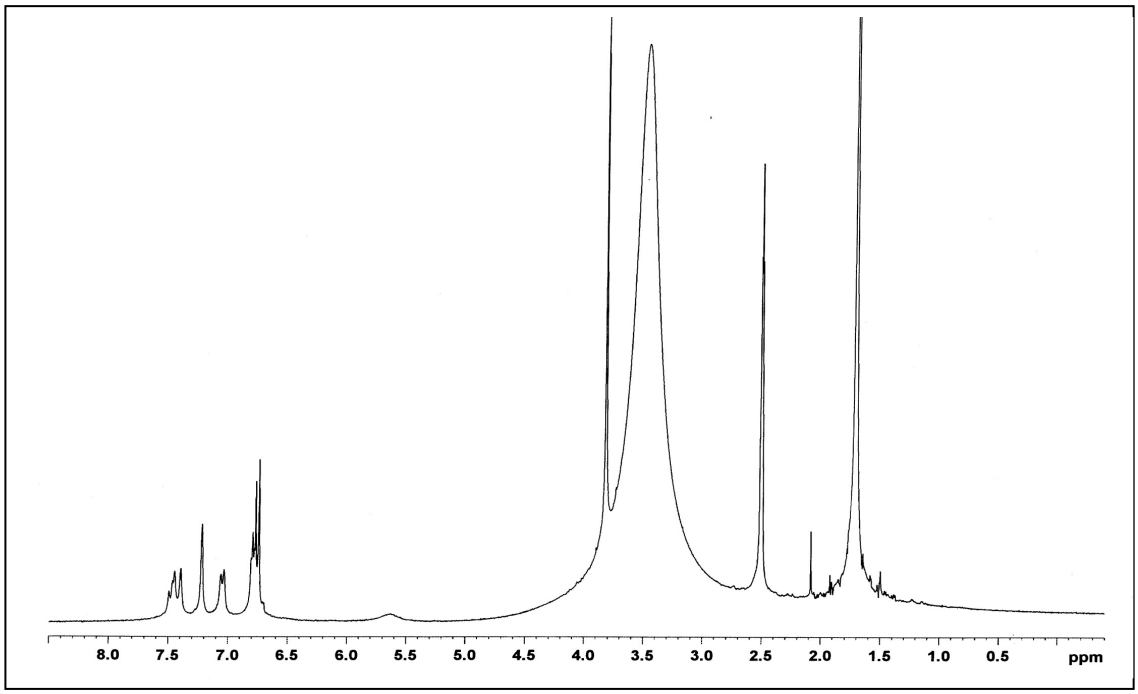

Figure 52 ^{1}H NMR spectrum of curcumin-Pb^{2+} in d_6-DMSO

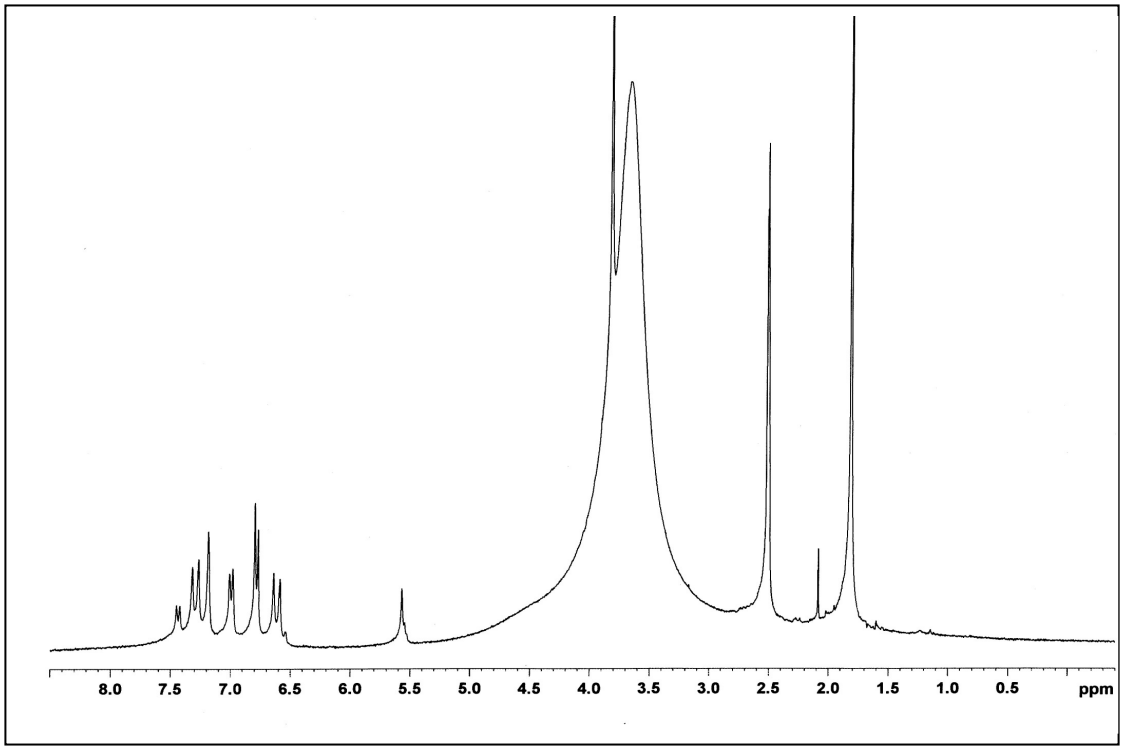

Figure 53 ^{1}H NMR spectrum of curcumin-Mg^{2+} in d_6-DMSO

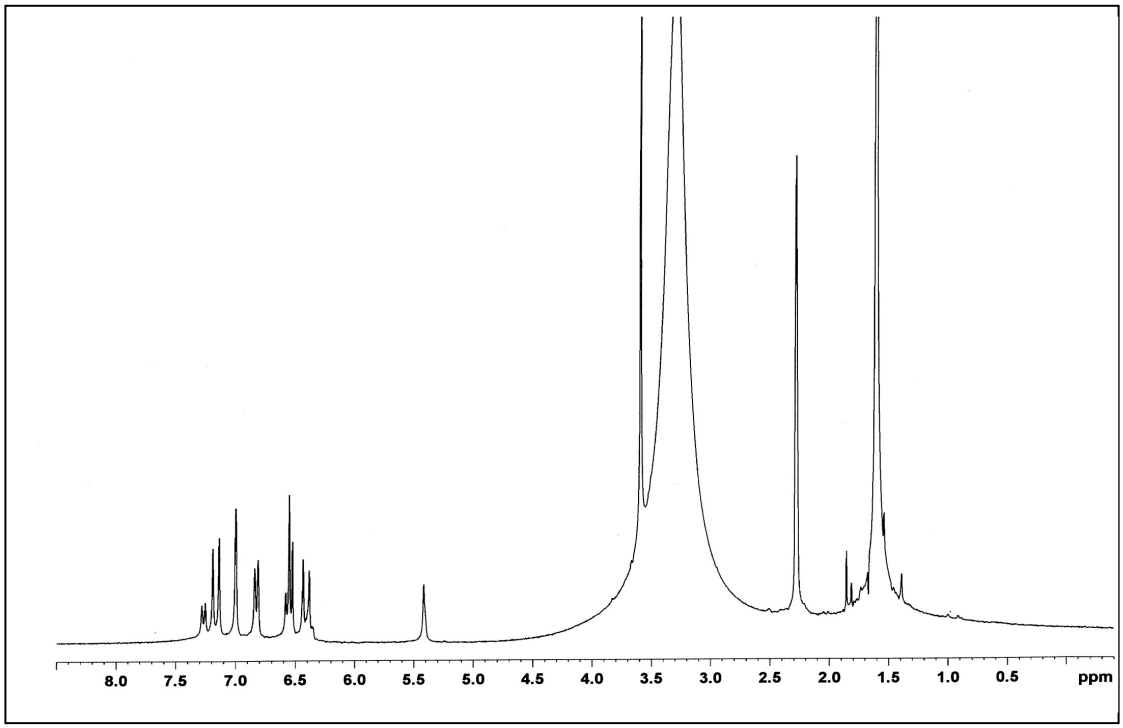

Figure 54 ^{1}H NMR spectrum of curcumin-Zn^{2+} in d_6-DMSO

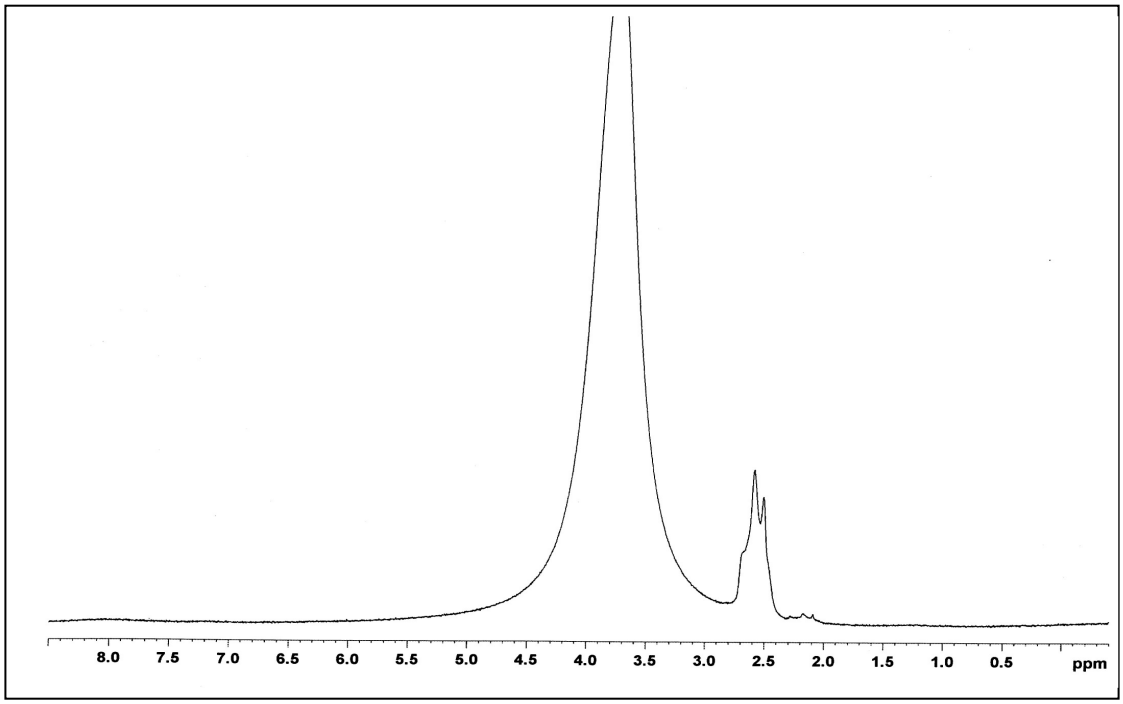

Figure 55 ^{1}H-NMR spectrum of curcumin-Co^{2+} in d_6-DMSO

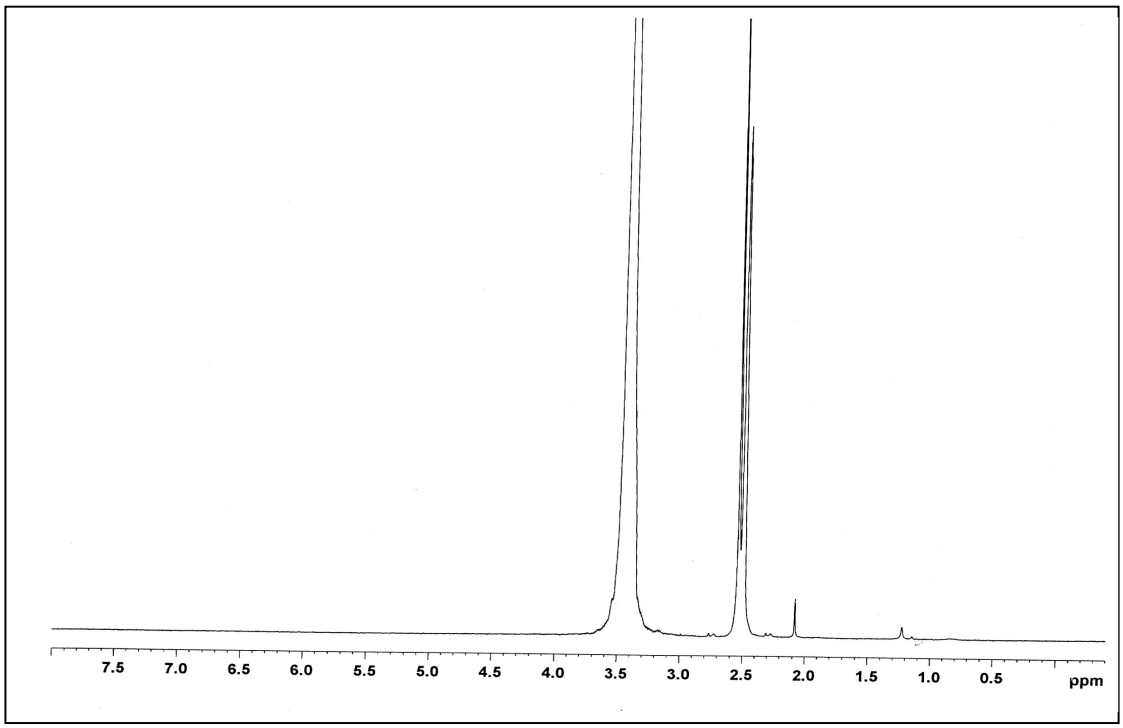

Figure 56 ^{1}H NMR spectrum of curcumin-Cu^{2+} in d_6-DMSO

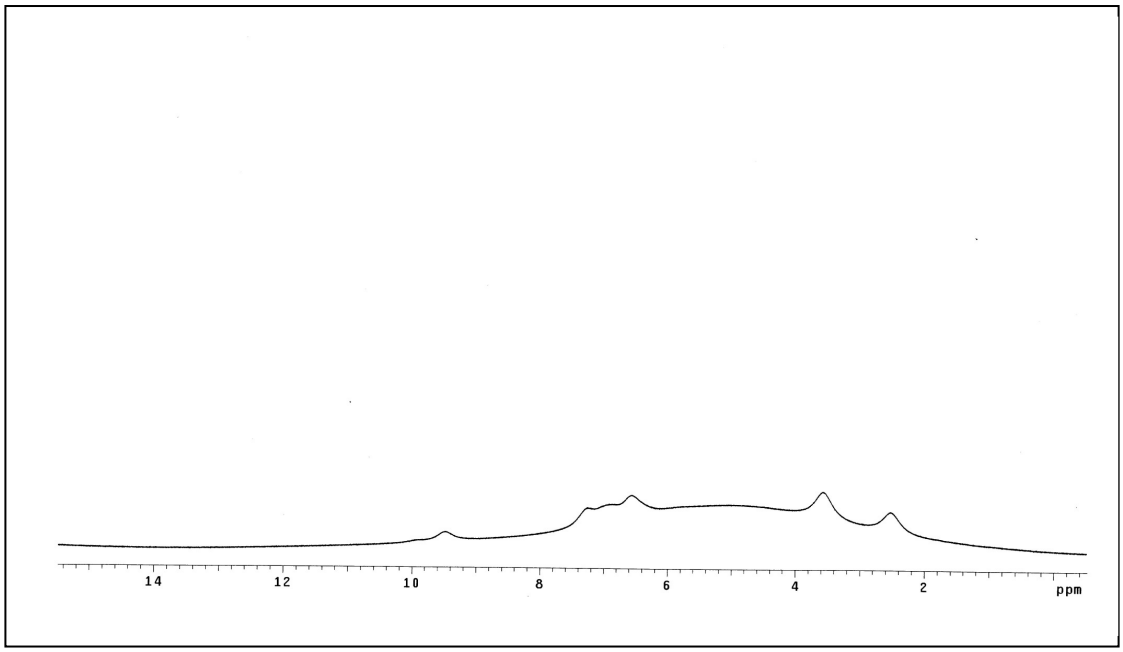

Figure 57 ^{1}H NMR spectrum of curcumin-Mn^{2+} in d_6-DMSO

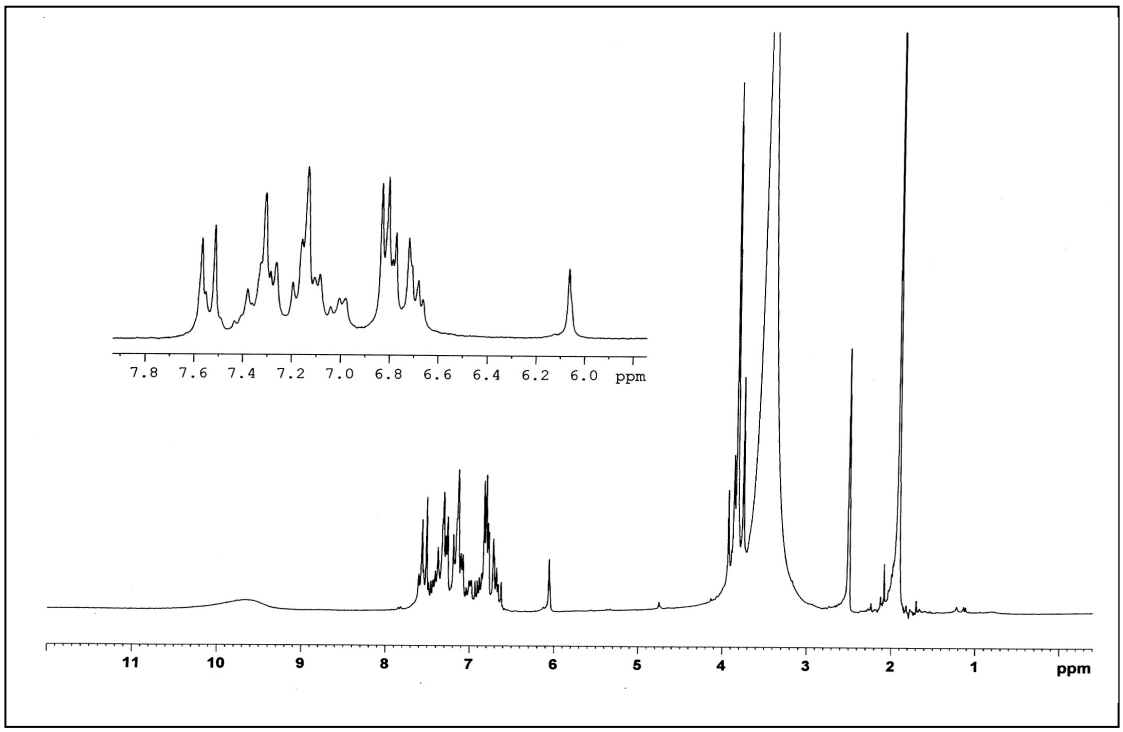

Figure 58 ^{1}H NMR spectrum of curcumin-Hg^{2+} in d_6-DMSO

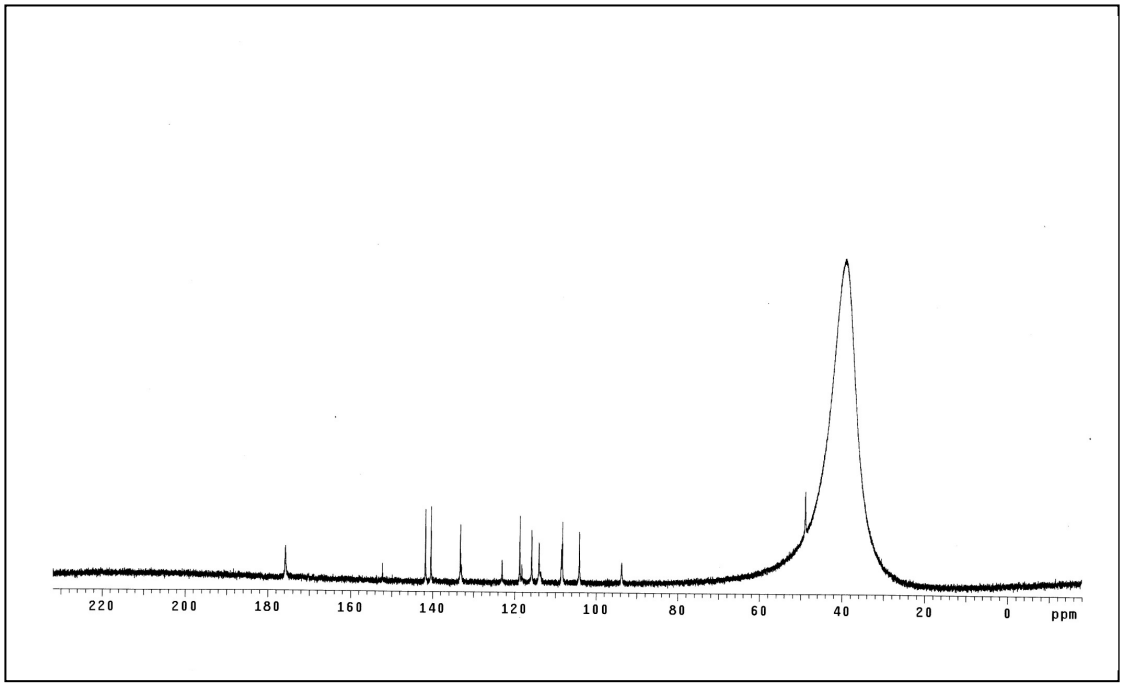

Figure 59 ^{13}C NMR spectrum of curcumin-Mn^{2+} in d_6-DMSO

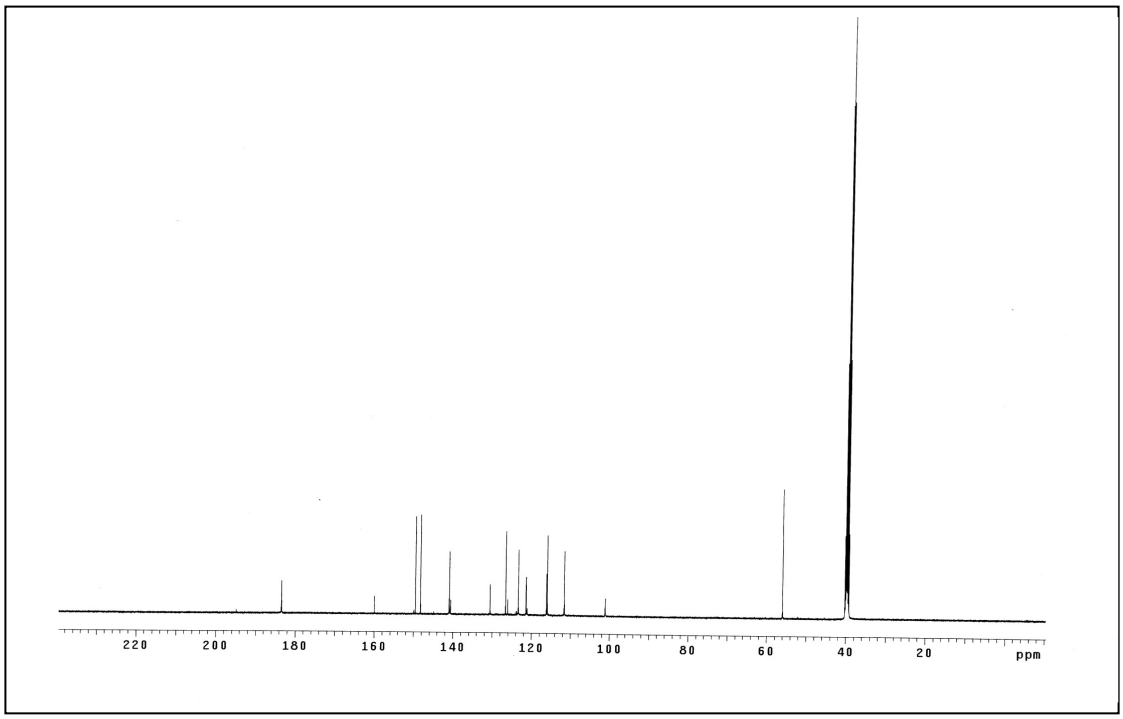

Figure 60 ^{13}C NMR spectrum of curcumin-Hg^{2+} in d_6-DMSO

3.3.3 NMR spectroscopy of acetylacetone

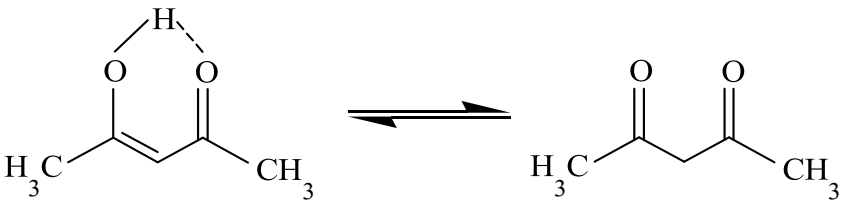

Figure 61 Keto-enol equilibrium of acetylacetone molecule.

Table 10 ^{1}H NMR spectroscopic data of acetylacetone

H-position	^{1}H NMR	
	δ(ppm)	Number of H
CH_3	2.2	3
CH_2 (keto form)	3.6	2
CH	5.7 (s)	1
OH (enol form)	15.5 (s)	1

The ^{1}H NMR spectral data of acetylacetone were in two solvents ($CDCl_3$ (weak polarity) and d_6-DMSO (strong polarity)) are summarized in Table 10. The resonance due to the OH proton appeared at 15.5 ppm. The methyl and methine signals of the acetylacetone moiety appeared as singglets at 2.2 and 5.7 ppm, respectively. The highest field signal was assigned to methyl group. The ^{1}H NMR spectra of acetylacetone in $CDCl_3$ and d_6-DMSO are shown in Figure 62 and 63.

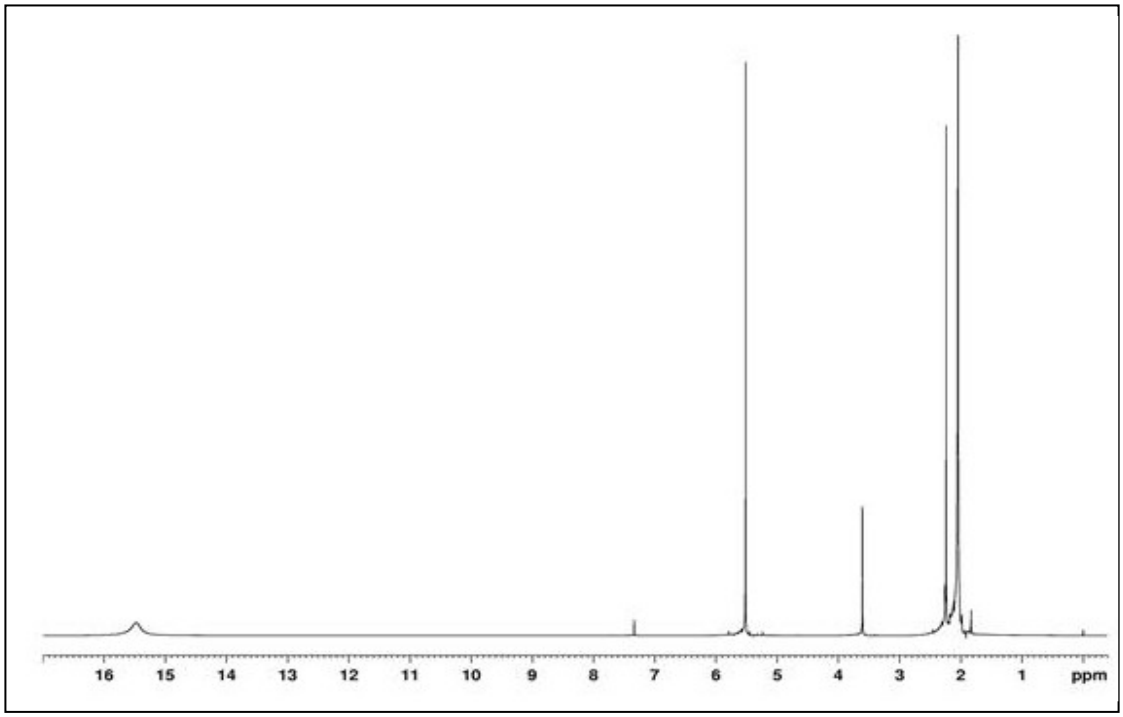

Figure 62 ^{1}H NMR spectrum of acetylacetone in $CDCl_3$

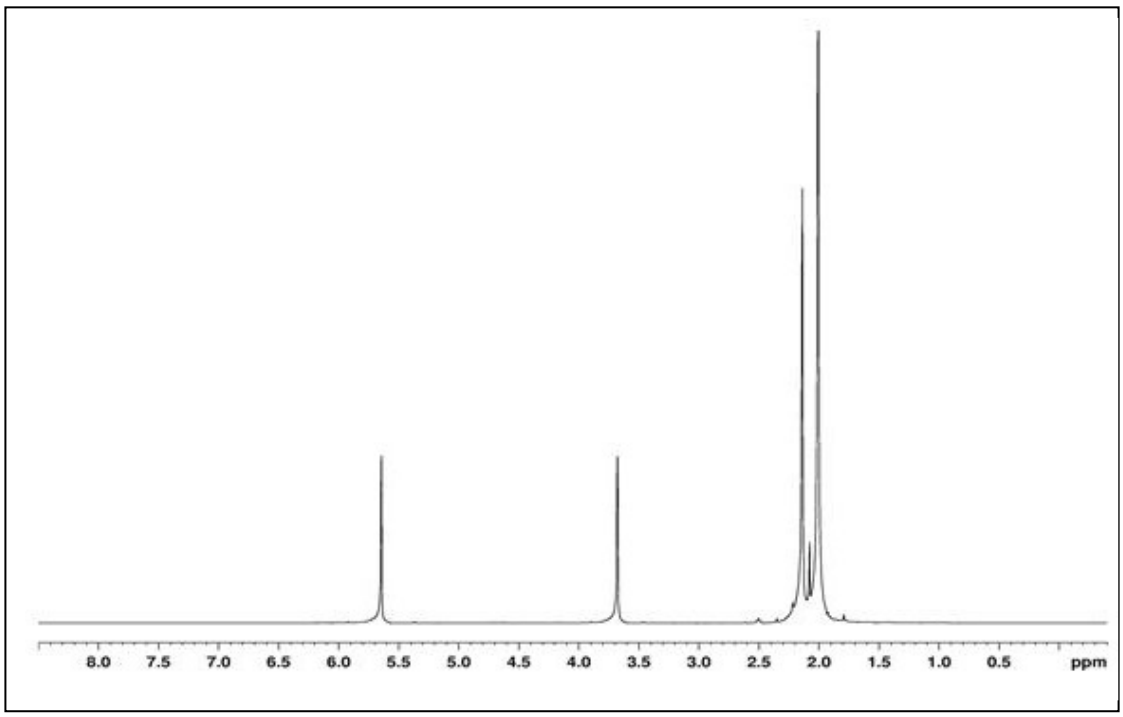

Figure 63 ^{1}H NMR spectrum of acetylacetone in d_6-DMSO

3.3.3 NMR spectroscopy of acetylacetone and metal ions in d_6-DMSO (Pb^{2+}, Hg^{2+})

In the ^1H NMR of Pb^{2+}-acetylacetone system, the singlets of CH and CH_3 protons (Figure 64) did not shift but in the Hg^{2+}-acetylacetone system (Figure 65) these protons showed upfield shift.

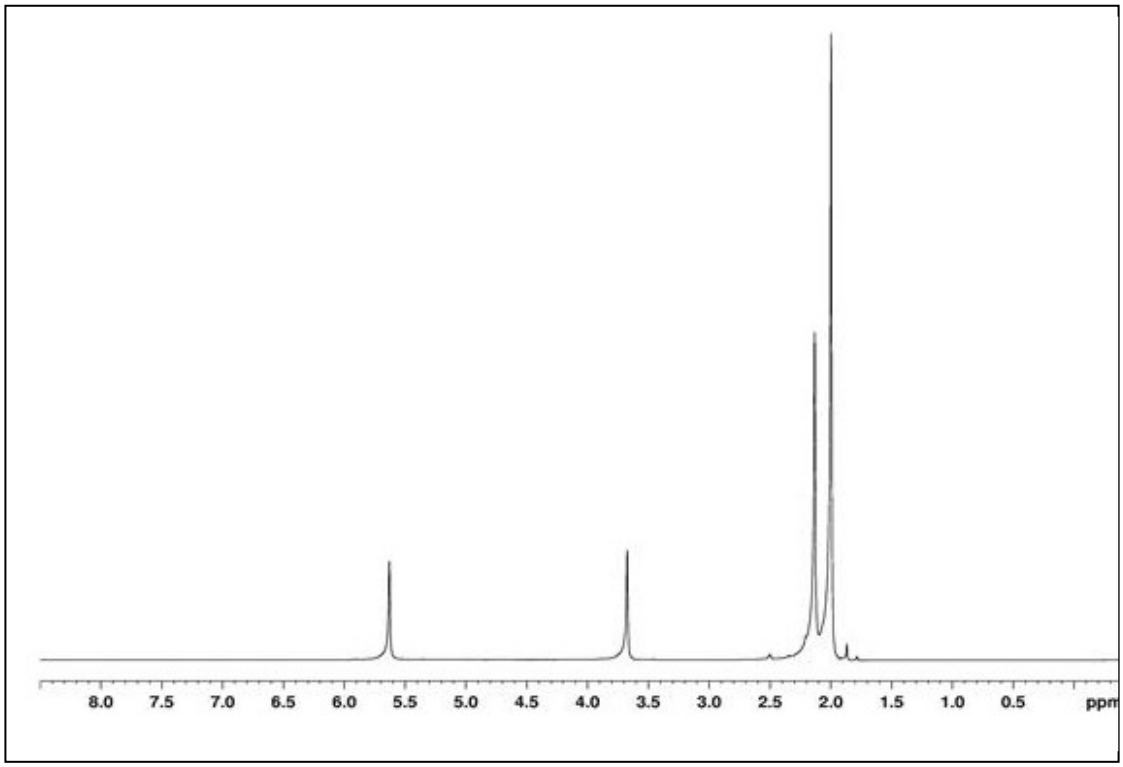

Figure 64 ^1H NMR spectrum of Pb^{2+}-acetylacetone system

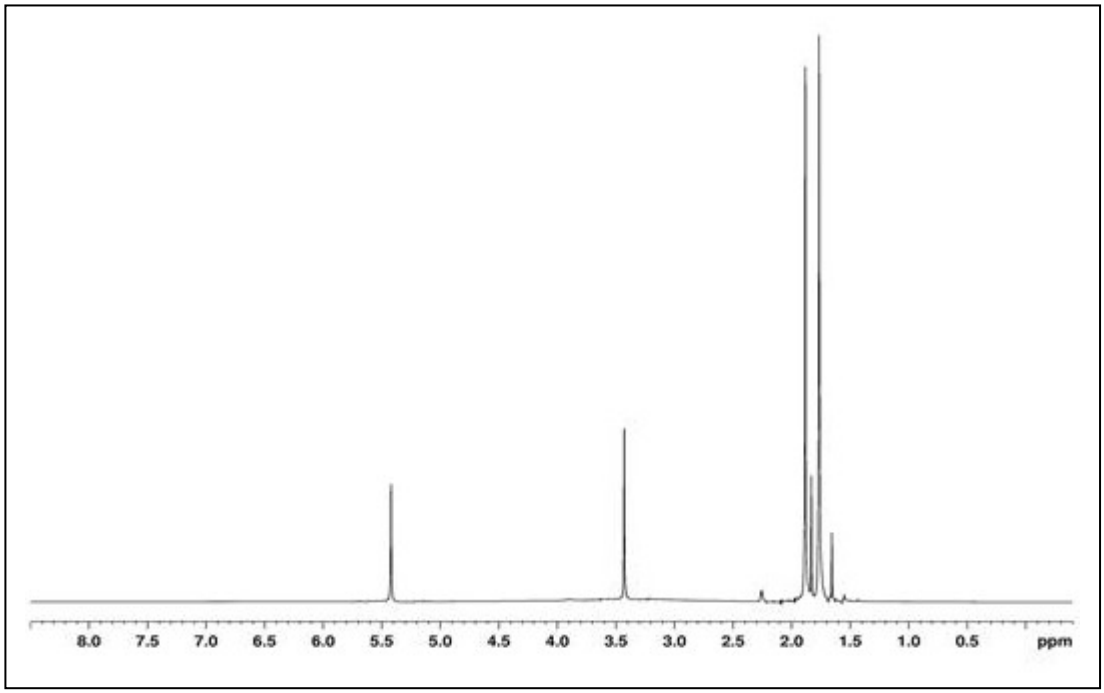

Figure 65 ^{1}H NMR spectrum of Hg^{2+}-acetylacetone system

3.4 The physical properties of curcumin and curcumin metal complexes

The physical properties of curcumin and curcumin metal complexes are listed in Table 11

Table 11 The physical properties of curcumin, curcumin-Pb^{2+} and curcumin-Cu^{2+} complexes

Substance	Physical properties		
	Appearance	Color	Melting points (°C)
curcumin	solid (powder)	bright yellow	183
cucumin-Pb^{2+}	solid (powder)	reddish-brown	> 300
cucumin-Cu^{2+}	solid (powder)	greenish-brown	> 300

The melting point of curcumin is 183°C while the melting points of the two products were indeterminable even up to 300 °C. In its normal form curcumin is a yellow powder and very soluble in organic solvents such as acetone, ethanol, DMSO and dimethyl formamide. The solubility of curcumin in these solvents is approximately 1 mg/ml, except in acetone which is at least 20 mg/ml. The solubility of 10 mg of the cucumin-Pb^{2+} and cucumin-Cu^{2+} complexes was tested in 10 ml of various solvents. The results showed that the complexes were slightly soluble in MeOH, EtOH and acetone but insoluble in water, toluene, hexane and CCl_4. It was completely soluble in NaOH solution.

3.4.1 Infrared spectroscopy

Infrared spectroscopy is a technique used for studying the functional groups of compounds. Infrared spectra were collected by using KBr pellets in the range 4000-370 cm^{-1}. The important vibrational frequencies are C=C, C=O and O-H stretching modes in curcumin.

Infrared spectroscopy of curcumin and complexes

The infrared spectroscopic data of curcumin and complexes are listed in Table 12.

Table 12 Infrared spectroscopic data of the curcumin and curcumin complexes

Vibration modes	Frequencies (cm^{-1})		
	curcumin	curcumin-lead	curcumin-copper
O-H stretching	3511	3445	3425
ν_{C-H}	3000-2930	2928-2822	2999-2832
$\nu_{C=O}$	1628 1600	1621 1582	1618 1590
$\nu_{C=C}$	1510	1491	1503
ν_{C-O} (in phenol)	1280	1277	1277
ν_{C-O} (in OCH_3)	1030	1027	1028
ν_{C-H}	975	975	970

The infrared spectra of the curcumin-lead complex and curcumin-copper complex are compared with curcumin as shown in Figure 66 and 67. Curcumin shows a strong sharp O-H stretching at 3511 cm^{-1}, probably ascribed to the hydroxyl group, and a medium-to-broad O-H stretching indicating strong hydrogen bonding at 3401 cm^{-1} ascribed to the hydrogen-bonded enol form of the β-diketone moiety (Daniel, *et al*., 2004). The metal derivatives show band with shifts to lower wavelengths (3445 cm^{-1} for lead, and 3425 cm^{-1} for copper) but the sharp O-H band disappears. Curumin possesses two strong carbonyl stretching at 1628 and 1600 cm^{-1}. The infrared spectra of both the lead and copper complexes are identical, suggesting they may share common structure when bonded to curcumin. The two carbonyls shift to lower wavenumber (1621 and 1582 cm^{-1} for lead, and 1618 and 1590 cm^{-1} for copper) and also the shift of ν(C-O) to 1277 cm^{-1} for both complexes.

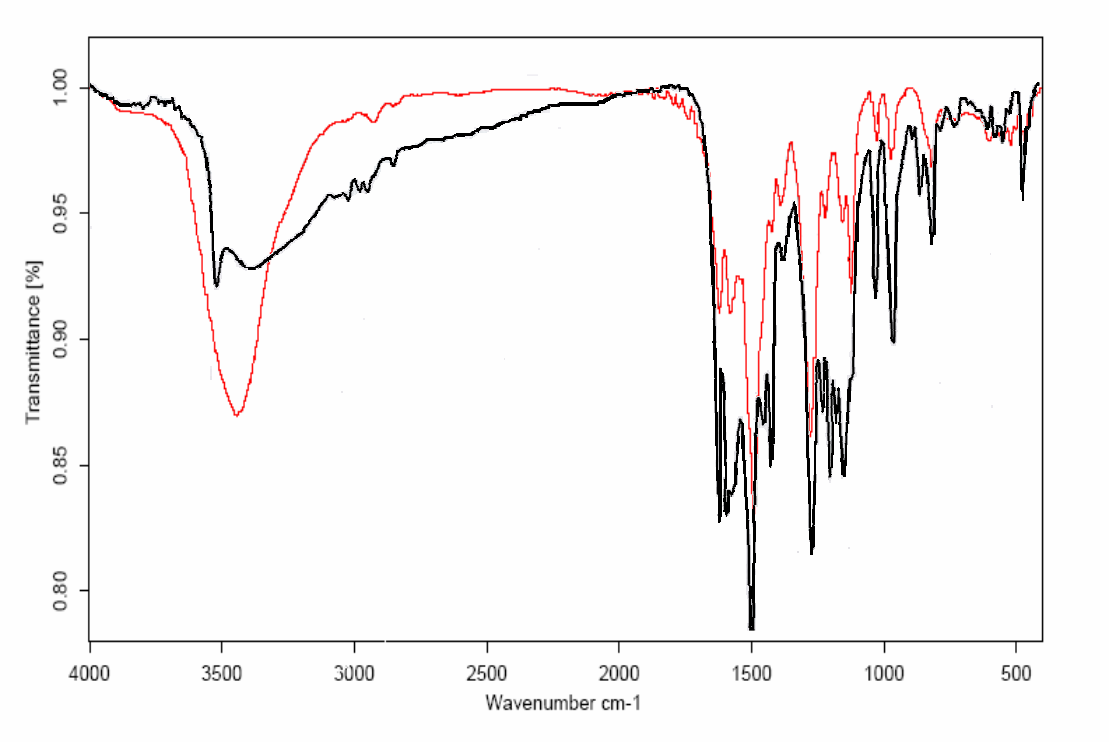

Figure 66 Infrared spectra of the curcumin–lead complex (—), and curcumin(—).

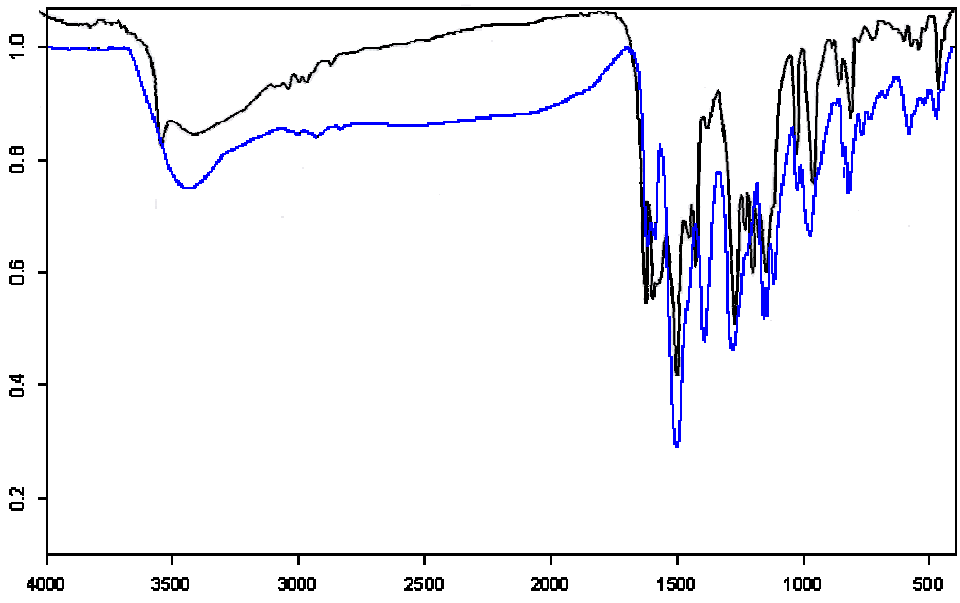

Figure 67 Infrared spectra of the curcumin-copper complex (—), and curcumin (—)

3.4.3 X-ray fluorescence spectrometry

X-ray fluorescence is one of the most widely used of all analytical methods for qualitative identification of element having atomic numbers greater than oxygen (>8). In addittion, it is often employed for semi-quantitative or quantitative element analyses as well.

The XRF spectrum of the precipitate obtained from reaction between curcumin and lead is shown in Figure 68 and likewise with copper in Figure 69. The presence of metal is clearly seen in each spectrum indicating that Pb and Cu are the main compositions of each residue.

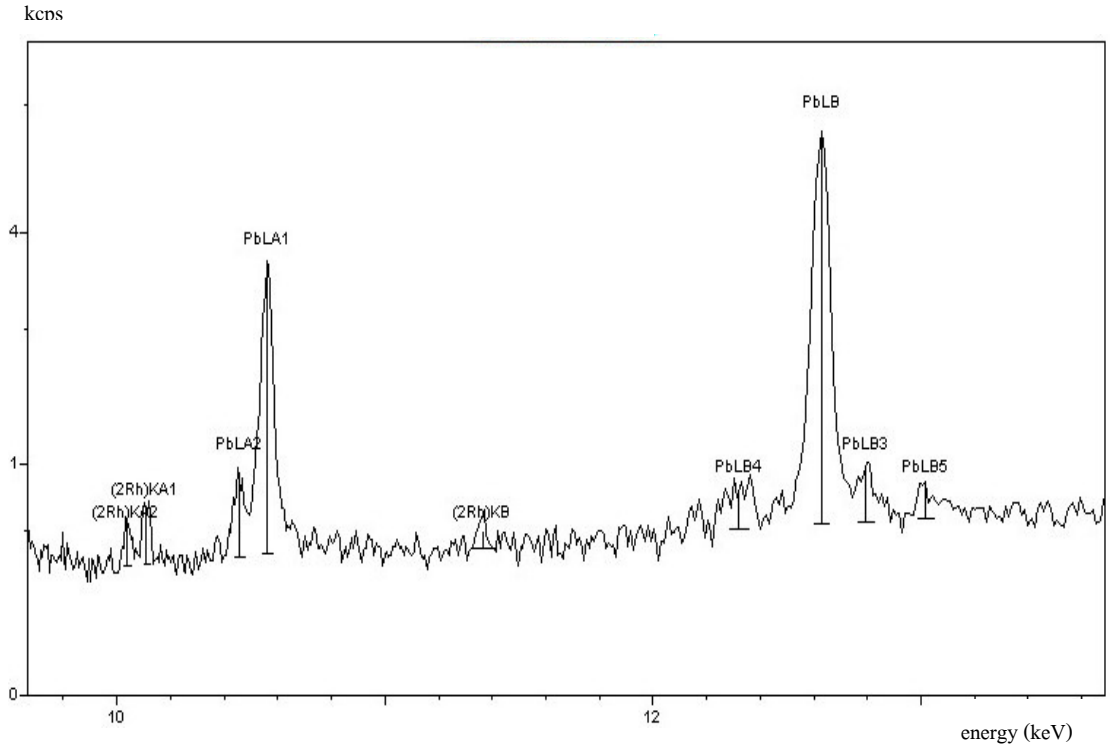

Figure 68 XRF spectrum of curcumin-lead complex

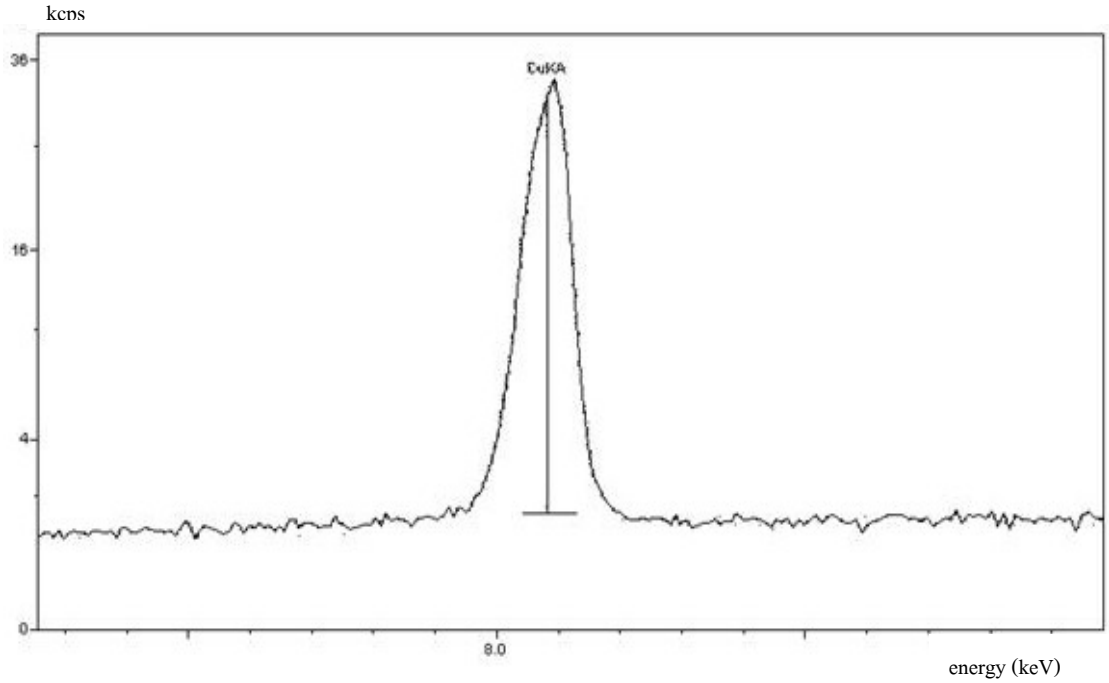

Figure 69 XRF spectrum of curcumin-copper complex